HMG Advance Access published April 30, 2014

Human Molecular Genetics, 2014 **1–18**
doi:10.1093/hmg/ddu166

Progressive axonal transport and synaptic protein changes correlate with behavioral and neuropathological abnormalities in the heterozygous Q175 KI mouse model of Huntington's disease

Gaynor A. Smith, Emily M. Rocha, Jesse R. McLean, Melissa A. Hayes, Sarah C. Izen, Ole Isacson and Penelope J. Hallett*

McLean Hospital/Harvard Medical School, Neuroregeneration Research Institute and Laboratories, Belmont, MA, USA

Received February 17, 2014; Revised March 31, 2014; Accepted April 7, 2014

A long-term goal of modeling Huntington's disease (HD) is to recapitulate the cardinal features of the disease in mice that express both mutant and wild-type (WT) huntingtin (Htt), as HD commonly manifests as a heterozygous condition in humans, and loss of WT Htt is associated with loss-of-function. In a new heterozygous Q175 knock-in (KI) mouse model, we performed an extensive evaluation of motor and cognitive functional deficits, neuropathological and biochemical changes and levels of proteins involved in synaptic function, the cytoskeleton and axonal transport, at 1–16 months of age. Motor deficits were apparent at 6 months of age in Q175 KI mice and at that time, postmortem striatal gamma-aminobutyric acid (GABA) levels were elevated and mutant Htt inclusions were present throughout the brain. From 6 months of age, levels of proteins associated with synaptic function, including SNAP-25, Rab3A and PSD-95, and with axonal transport and microtubules, including KIF3A, dynein and dynactin, were altered in the striatum, motor cortex, prefrontal cortex and hippocampus of Q175 KI mice, compared with WT levels. At 12–16 months of age, Q175 KI mice displayed motor and cognitive deficits, which were paralleled at postmortem by striatal atrophy, cortical thinning, degeneration of medium spiny neurons, dense mutant Htt inclusion formation, decreased striatal dopamine levels and loss of striatal brain-derived neurotrophic factor (BDNF). Data from this study indicate that the heterozygous Q175 KI mouse represents a realistic model for HD and also provides new insights into the specific and progressive synaptic, cytoskeletal and axonal transport protein abnormalities that may accompany the disease.

INTRODUCTION

Huntington's disease (HD) is an autosomal dominant inherited neurodegenerative disorder, caused by a mutation that expands a CAG repeat motif in exon 1 of the huntingtin (Htt) gene. The disease usually manifests in adulthood, where patients develop early neuropsychiatric problems and chorea. Homozygosity is rare in humans with HD, and the majority of patients have a single allele containing the expanded CAG mutation. Therefore, the goal of preclinical research is to test potential therapeutic strategies in models that closely mimic biological changes in the presence of both normal and mutant Htt. Indeed, a conditional knockout of normal Htt in mice causes progressive neurodegeneration and highlights the critical role for WT Htt in neuron survival (1). *In vivo* modeling of HD using heterozygous knock-in (KI) mice has previously been challenging owing to their subtle phenotypes, and hence, the majority of mutant Htt KI models used to date are homozygous (2–5). Q175 KI mice are a novel HD model that recapitulate the heterozygosity of human HD and provide an opportunity to identify progressive functional and neurodegenerative changes. Given our previous work showing that early synaptic, cytoskeletal and axonal

*To whom correspondence should be addressed at: Neuroregeneration Laboratories, Mailman Research Center, Rm. 125, McLean Hospital/Harvard Medical School, 115 Mill Street, Belmont, MA 02478, USA. Tel: +1 6178552082; Email: phallett@mclean.harvard.edu

transport protein alterations precede overt neuronal degeneration in a progressive rodent model of Parkinson's disease (6), we hypothesized that changes in similar systems would precede or correlate with behavioral and neuropathological abnormalities in the Q175 KI model of HD. We have now performed an extensive evaluation of behavioral, pathological and degenerative changes, and alterations to key intracellular proteins involved in synaptic maintenance and axonal transport, in Q175 KI mice.

The neuropathological changes observed in human HD brains at post-mortem (grades 1–4) closely correlate with the extent of clinical disability (7). However, no pathological changes are found in grade 0 brains, immediately after clinical diagnosis (7), suggesting that pre-degenerative processes also affect symptomology. 95% of neurons in the caudate nucleus are lost at grade 4 (7), and severe atrophy of the cerebral cortex is observed (8,9). At grade 1, mutant Htt N-terminal fragments initially accumulate in the cytoplasm of neurons within the corticostriatal tract, and during disease progression, these form intra-nuclear inclusions (10). Soluble and misfolded Htt causes numerous abnormal direct and indirect protein interactions, which result in pathway-specific gain-of-function and loss-of-function effects in cellular processes (11). In HD patients and in mouse models of the disease, fast axonal transport, synaptic vesicle release, energy homeostasis, the ubiquitin–proteasome system and endosomal recycling pathways are dysregulated (12–16). Under normal conditions, vesicles, mitochondria and lysosomes move 50–400 mm per day within the neuron, shuttling from + to − ends at ∼0.3 μm/s, reviewed in (16). Vesicles containing synaptic proteins also move from the endoplasmic reticulum (ER) to the terminals, for synaptic spine maintenance *in vivo*, and hence under conditions of disrupted organelle transport, dendritic spines are lost (17). *In vitro* experiments show that Htt is associated with vesicle membranes in the cytoplasm, controlling both anterograde and retrograde transport on microtubules (18–21). Mutant Htt prevents adequate protein and organelle delivery, by fast axonal transport, leading to vesicle accumulation in the axon, demonstrated in the squid giant axoplasm, *Drosophila melanogaster* and in transgenic HD mouse model systems (22–25). It is likely that aggregated insoluble mutant Htt also physically inhibits vesicle motility at latter stages, as swollen organelles are seen in close proximity to Htt aggregates, in a HD mouse model (26). *In vitro* paradigms reveal that mutant Htt causes microtubule deacetylation and detachment of the fast-axonal vesicle-carrying motor proteins dynein and kinesin (27), resulting in the loss of retrograde and anterograde transport, respectively. The binding of vesicles to dynein and kinesin, *in vitro*, is further perturbed by the loss of Htt binding to HAP-1 (28). These motor proteins are essential to the maintenance of medium spiny neurons (MSNs) and loss-of-function mutations in dynein cause decreased neuronal outgrowth *in vitro* and striatal atrophy *in vivo* (29). Brain-derived neurotrophic factor is transported in vesicles from the cortex to nerve terminals in the striatum, via attachment to dynactin and dynein complexes. The decrease in BDNF and transport problems of the BDNF receptor, TrkB, seen in HD patients and HD mouse models are considered a causative mechanism of degeneration (15,30–32). It has recently been found that human HD iPSC-derived neurons are also susceptible to BDNF withdrawal (33). The impact, timing and specificity of key axonal transport, cytoskeletal and neurotrophic factor-related protein changes in cortical, hippocampal and striatal neuron populations has yet to be elucidated in HD pathogenesis.

Small Rab GTPases, which provide the rate-limiting step for vesicle trafficking and vesicle fusion, have also been implicated in the pathogenic phenotype of HD mouse models (17), HD patient fibroblasts (34) and cellular dysfunction in other neurodegenerative diseases (35,36). Mutant Htt interacts with Rab11 to cause the impaired exit from recycling endosomes in a KI mouse model of HD (37). As a consequence, Rab11-positive vesicles containing spine-maintaining cargo fail to be delivered in mutant Htt-expressing cells, resulting in synaptic degeneration (34). The protein homeostasis of other Rab GTPases, of which there are >70 subtypes in humans, is much less understood in the context of HD.

Inadequate maintenance of the synaptic spine results in altered synaptic plasticity, which can be measured in the corticostriatal tract and hippocampus of HD patients (12) and transgenic HD mouse models (13,38–42). Dissociating between regional changes of pre- and post-synaptic proteins, and discerning which soluble *N*-ethylmaleimide-sensitive factor attachment protein receptor (SNARE) complex proteins are most effected in HD over time, in conjunction to neurotransmitter changes, is paramount to understanding the origins of abnormal synaptic plasticity changes.

In the current study, we therefore investigated synaptic, cytoskeletal, axonal transport, neurotransmitter and BDNF protein changes, in the novel Q175 KI mouse model of HD, in parallel to assessing disease progression by different output measures. We show that a KI expansion of 175 CAG repeats into the Htt gene, on a single allele, results in a robust heterozygous mouse model of HD, which exhibits motor deficits and inclusion pathology by 6 months. We have confirmed existing pathological and biochemical changes found in HD patients and have identified novel protein alterations. The Q175 KI model recapitulates both the phenotype and WT/mutant Htt heterozygosity of the human condition, and Q175 KI mice are well suited for testing novel therapeutic interventions for use in HD.

RESULTS

Progressive behavioral deficits in Q175 KI mice

Behavioral analyses of spontaneous behavior, motor coordination, working memory and nesting were performed in Q175 KI mice at 1, 6, 12 and 16 months of age. Some of these functional deficits were exacerbated with age in Q175 KI mice. In the cylinder test, the number of hindlimb steps, forelimb steps, rears and time spent grooming were assessed. Q175 KI mice displayed an increase in the number of hindlimb steps at 1 month of age ($T_{1,46} = 2.63, P < 0.05$) and a decrease in the time spent grooming at 6 months of age ($T_{1,40} = 2.60$, $P < 0.05$), compared with age-matched WT littermates (Fig. 1A and B). Hindlimb steps were also increased in Q175 KI mice at both 12 months of age ($T_{1,36} = 2.60$, $P < 0.05$; Fig. 1C) and 16 months ($T_{1,23} = 3.02, P < 0.01$; Fig. 1D). Q175 KI mice showed a progressive increase in forelimb steps with age; forelimb steps did not differ between Q175 KI mice and WT mice at 1 and 6 months, yet were increased in Q175 KI mice at 12 months ($T_{1,36} = 2.37, P < 0.05$; Fig. 1C), and 16 months ($T_{1,23} = 2.59$,

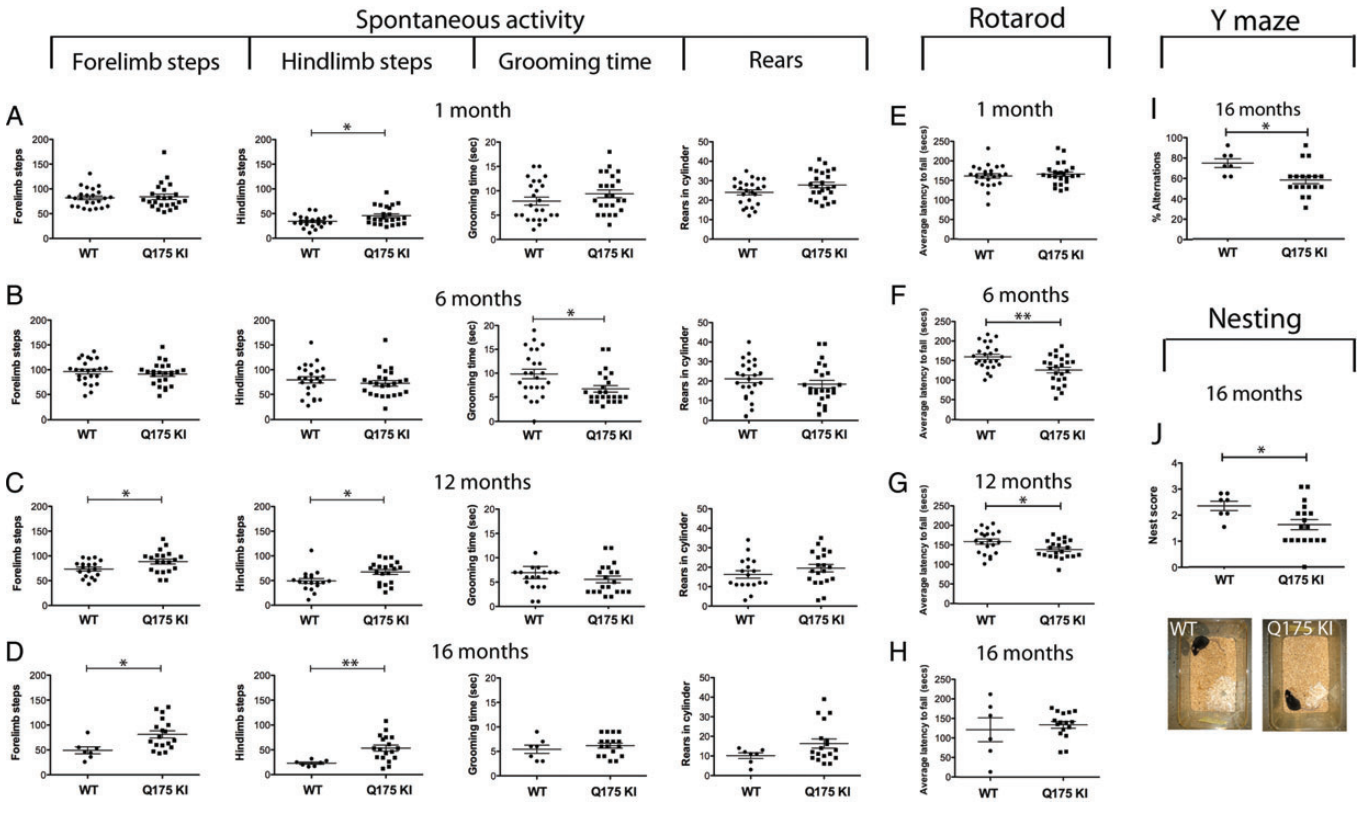

Figure 1. Progressive behavioral deficits in heterozygous Q175 knock-in (Q175 KI) mice. Heterozygous Q175KI and age-matched WT littermate mice at 1, 6, 12 and 16 months of age were assessed for spontaneous activity using the cylinder test (**A**–**D**). Forelimb steps, hindlimb steps, time spent grooming and rearing were measured. Forelimb steps were increased in Q175 KI mice compared with WT littermate mice at 12 and 16 months of age (C and D), and the number of hindlimb steps was increased in Q175KI mice at 1, 12 and 16 months (A, C and D). Motor coordination deficits in Q175KI and WT littermate mice were assessed using the accelerating rotarod (**E**–**H**). Q175 KI mice showed a decreased latency to fall on the accelerating rotarod at 6 and 12 months (F–G). Working memory was measured in Q175KI and WT littermate mice using the Y-maze (**I**). Percent alternation was decreased in the Y-maze in Q175 KI mice at 16 months of age (I). Motivational behavior was assessed by a test for nesting deficits (**J**). Q175 KI mice built less elaborate cotton nests at 16 months (J). Significance is annotated at $^{*}P < 0.05$ compared with age-matched WT littermate mice, unpaired *T*-tests. $N = 8$–24/group. Graphs are expressed as mean ± SEM.

$P < 0.05$; Fig. 1D). No motor coordination deficits on the accelerating rotarod, as determined by a decreased latency to fall, were observed at 1 month of age. However, Q175 KI mice developed rotarod deficits at 6 months ($T_{1,46} = 3.01, P < 0.01$), which persisted at 12 months of age ($T_{1,40} = 2.49$, $P < 0.05$), compared with age-matched littermate WT mice (Fig. 1F and G). Q175 KI mice also showed a decreased alternation on the Y-maze test ($T_{1,23} = 2.58, P < 0.05$) and displayed a decreased capacity to build cotton nests ($T_{1,23} = 2.49$, $P < 0.05$) at 16 months (Fig. 1I and J). Deficits on the Y-maze and the nest-building tests were not observed at 12 months of age (data not shown). Prior to behavioral testing, the weight of each mouse was recorded. Q175 KI mice failed to gain weight at 12 and 16 months in contrast to age-matched WT littermates (Supplementary Material, Fig. S1).

Age-dependent Htt inclusion formation and brain atrophy

The progressive formation of intra-neuronal nuclear protein aggregates of mutant Htt is a pathological hallmark in patients with HD (10) and in transgenic HD mouse models (3,43–45). We investigated the expression pattern of mutant Htt inclusions throughout the brain of Q175 KI mice at 1, 6, 12 and 16 months of age. DAB immunostaining using an EM48 antibody for mutant Htt (46) showed that aggregates were present in Q175 KI mice by 6 months of age and that inclusions increased in number and density within the striatum, prefrontal cortex and motor cortex, progressively with age (Fig. 2A and Table 1). Semi-quantitative scores of mutant Htt inclusions, based on Bayram-Weston *et al.* (2,3,44,45), indicated that at 6 months, there were few inclusions in the lateral striatum, motor cortex, prefrontal cortex and piriform cortex. At 6 months, there was also diffuse nuclear staining in the amygdala, thalamus, hypothalamus, nucleus accumbens, sensory cortex, medial striatum and caudal striatum (Table 1). In contrast, there was no evidence of mutant Htt accumulation in the septum or substantia nigra at 6 months (Table 1). In 12-month-old Q175 KI mice, mutant Htt inclusions were frequent and dense in the medial striatum, lateral striatum, motor cortex, prefrontal cortex, sensory cortex and piriform cortex, and diffuse nuclear staining was apparent in all other regions of interest (Table 1). At 16 months, Q175 KI mice showed dense mutant Htt inclusions throughout the brain, yet only few inclusions were observed in the *s. nigra* (Table 1).

HD is associated with selective neuronal vulnerability and loss in the caudate-putamen (striatum) and cerebral cortex, resulting in atrophy that closely tracks the disability of the disease in patients (47). We therefore evaluated striatal volume and cortical thickness in Q175KI mice. Striatum

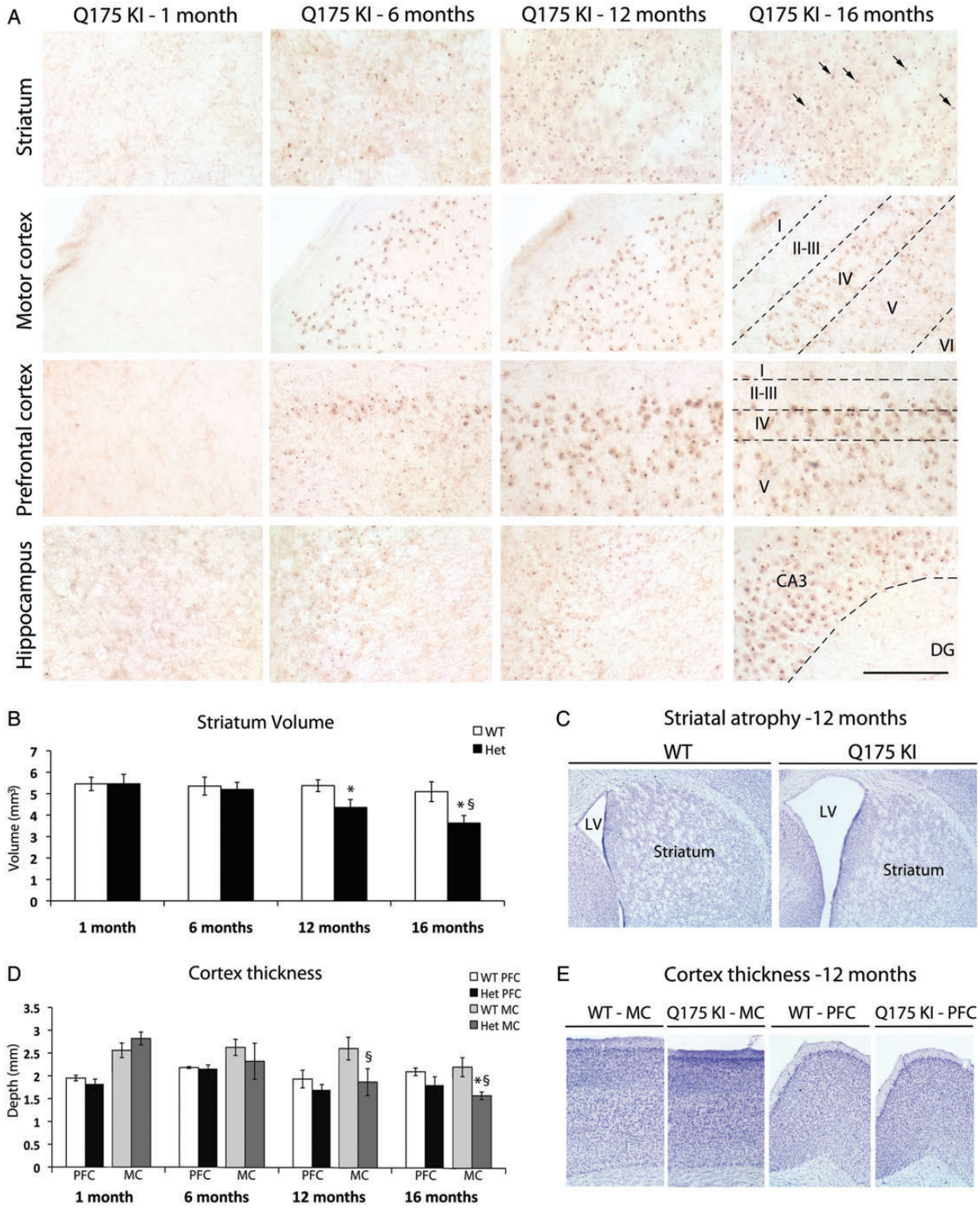

Figure 2. Accumulation of mutant huntingtin inclusions and atrophy of the striatum and motor cortex in heterozygous Q175 knock-in (Q175 KI) mice. Immunolabeling for mutant huntingtin in Q175KI mice shows mutant huntingtin-positive inclusions in the striatum, motor cortex, prefrontal cortex and hippocampus at 6, 12 and 16 months of age (**A**). No inclusions were detected in Q175KI mice at 1 month of age. Striatal volume (**B** and **C**) and cortical (motor and prefrontal) thickness (**D** and **E**) was measured in Q175KI and WT mice at 1, 6, 12 and 16 months of age in Nissl-stained sections. Striatal volume was decreased in Q175 KI mice at 12 months of age in comparison with age-matched WT mice (B), and motor cortex volume was reduced in 12- and 16-month-old Q175 KI mice in comparison with Q175 KI mice at 1 month of age and in 16-month-old mice compared with age-matched WT littermates (D). Representative photomicrographs are shown from 12-month-old mice (C and E). Photomicrographs are annotated with arrows showing mutant Htt inclusions, and specific regions and cortical layers within the dashed lines in the 16-month column. Significance is annotated as $^{*}P < 0.05$ compared with WT mice of the same age and $^{\S}P < 0.05$ compared with Q175 KI at 1 month of age, two-way and MANOVAs with Dunnett's *post hoc* tests. $N = 8–12$/group. Abbreviation: lateral ventricle (LV). Graphs are expressed as mean ± SEM. Scale bar in Panel A = 100 μm.

Table 1. Regional specificity and distribution of mutant huntingtin inclusions in the brain of Q175 KI mice

Brain region	1 month	6 months	12 months	16 months
Striatum lateral	--	***/****	****	****
Striatum medial	--	**	****	****
Striatum rostral	--	*/**	***	****
Striatum caudal	--	*	***	****
Nucleus accumbens	--	**	***	****
Septum	--	--	**	***
Amygdala	--	*	**	***/****
Thalamus	--	*	**	***/****
Hypothalamus	--	*	**	***/****
Hippocampus	--	**	***	****
Motor cortex	--	***	****	****
Prefrontal cortex	--	***	****	****
Sensory cortex	--	**	***/****	****
Piriform cortex	--	***	****	****
Substantia nigra	--	--	*/**	*/**

Rating scale: --, absent; *, weak nuclear staining present; **, diffuse nuclear staining; ***, few/minimum inclusions; ****, many/dense inclusions.

volume, measured on Nissl-stained sections, was reduced in Q175 KI mice at 12 months ($F_{1,68} = 40.1$, $P < 0.05$) and 16 months of age ($F_{1,68} = 46.2$, $P < 0.05$) compared with age-matched WT littermate mice (Fig. 2B). Representative photomicrographs indicate that the reduced striatum volume was paralleled by an increase in the size of the lateral ventricle (LV) in 16-month-old mice (Fig. 2C). Motor cortex thickness in Q175 KI mice was decreased at 12 months of age ($F_{7,68} = 2.20$, $P < 0.05$) compared with Q175 KI mice at 1 month of age (Fig. 2D and E). In 16-month-old Q175 KI mice, motor cortex volume was further reduced compared with both age-matched WT littermate controls ($F_{7,68} = 2.22$, $P < 0.05$) and Q175 KI mice at 1 month of age ($F_{7,68} = 3.58$, $P < 0.05$) (Fig. 2D and E). In contrast, there was no change in the prefrontal cortex thickness with age (Fig. 2D and E).

Despite the widespread occurrence of mutant Htt inclusions and brain atrophy in Q175 KI mice at 12 months, this had little effect on the total levels of Htt. There was no difference in the levels of either total full-length Htt or N-terminal Htt fragments compared with levels in WT mice at 12 months of age in the striatum and motor cortex (Fig. 3A–D). There was also no difference in the levels of either total full-length Htt or N-terminal Htt fragments in the striatum of Q175 KI mice at 16 months (Supplementary Material, Fig. S5I and J).

Q175 KI mice developed an age-dependent decrease in DARPP-32 proteins levels (Fig. 4Ai–Dii). When quantified, there were no genotype-specific differences in DARPP-32 levels at 1 and 6 months. However, in 12-month, Q175 KI mice DARPP-32 levels were 44 ± 6% lower than age-matched WT levels ($U = 2.00, P < 0.05$) and at 16 months were 53 ± 9% lower than WT ($U = 1.00$, $P < 0.01$). In contrast, there were no changes in the intensity of TH staining of dopaminergic fibers that innervate the striatum in Q175 KI mice at any age (Fig. 4A–Diii). Stereological analysis revealed that Q175 KI mice also had a loss of MSNs at 16 months ($F_{1,68} = 38.7$, $P < 0.05$) compared with age-matched WT littermates (Fig. 4E), yet there was no change in tyrosine hydroxylase levels, as measured by optical density analysis (Fig. 4F). There was no significant difference between the number of NeuN-positive cells in the CA1 region of the hippocampus between Q175 KI mice ($10.14 \times 10^4 \pm 0.69$) and age-matched WT mice ($8.89 \times 10^4 \pm 0.72$) at 16 months. Similarly, there was also no difference in the number of NeuN-positive cells in the CA3 region of Q175 KI mice ($9.79 \times 10^4 \pm 1.37$) compared with WTs ($9.32 \times 10^4 \pm 0.78$). Nissl-stained sections from 12-month-old Q175 KI mice contained swollen cell bodies and a loss of Nissl in layers V–VI of the supplementary cortex, and in layers II–III of the motor cortices, compared with age-matched WT mice (Fig. 4G). No changes in Nissl staining were found in other anatomical regions of the Q175 KI mouse brain (data not shown) or in age-matched WT mice.

Progressive cytoskeletal, axonal transport and synaptic protein changes in Q175 KI mice

We have previously demonstrated in other progressive neurodegenerative disease models that an altered expression of synaptic, cytoskeletal and axonal transport proteins precede overt neuronal degeneration (6,35). We therefore measured cytoskeletal, axonal transport and synaptic protein expression in Q175 KI and WT littermate mice at 12 months of age (Figs 5 and 6), a time point when mice display a robust motor behavioral phenotype and have widespread mutant Htt accumulation, yet precedes a significant loss of MSNs.

At 12 months of age, the levels of structural, axonal transport and synaptic proteins were investigated in the striatum, motor cortex, prefrontal cortex and hippocampus (Figs 5 and 6). The cytoskeletal protein γ-tubulin was increased in the striatum ($U = 0.00$, $P < 0.01$) of 12-month-old Q175 KI mice (Fig. 5A and B), whereas α-tubulin was increased in the motor cortex ($U = 1.00$, $P < 0.05$) and hippocampus ($U = 1.00$, $P < 0.01$) compared with age-matched WT littermates (Fig. 5C, D, G and H). In contrast, there was no evidence of cytoskeletal changes in the prefrontal cortex (Fig. 5E and F), and β-tubulin remained unchanged in all regions. There was a reduction in the level of the anterograde transport motor protein KIF3A ($U = 2.00$, $P < 0.05$) in the motor cortex (Fig. 5C and D) and a reduction in both KIF3A ($U = 2.00$, $P < 0.05$) and KIF17 ($U = 3.00, P < 0.05$) in the hippocampus (Fig. 5G and H). Conversely, KIF17 was increased ($U = 2.00$, $P < 0.05$) in the prefrontal cortex (Fig. 5E and F). In addition, levels of KIF17 in the striatum and motor cortex of Q175 KI mice were positively correlated ($r = 0.82$, $P < 0.05$). Levels of KIF1A did not differ from WT counterpart levels in any region of interest. There was an increase in the levels of the retrograde transport proteins dynein ($U = 1.00$, $P < 0.01$) and dynactin ($U = 2.00$, $P < 0.05$) in the striatum of Q175 KI mice at 12 months of age (Fig. 5A and B), yet dynactin levels were reduced in the motor cortex ($U = 1.00$, $P < 0.05$; Fig. 5C and D). Dynactin was also increased in the prefrontal cortex ($U = 2.00$, $P < 0.05$) compared with WT littermate controls (Fig. 5E and F). Dynein and dynactin protein level increases were closely correlated to each other in the striatum ($r = 0.76$, $P < 0.05$, Supplementary Material, Table S1). Further, there was a negative correlation between dynein in the motor cortex and dynactin in the striatum ($r = -0.83$, $P < 0.05$, Supplementary Material, Table S2). There was a reduction in the mitochondrial and Golgi to ER-trafficking proteins, Tom20 ($U = 2.00$, $P < 0.05$) and

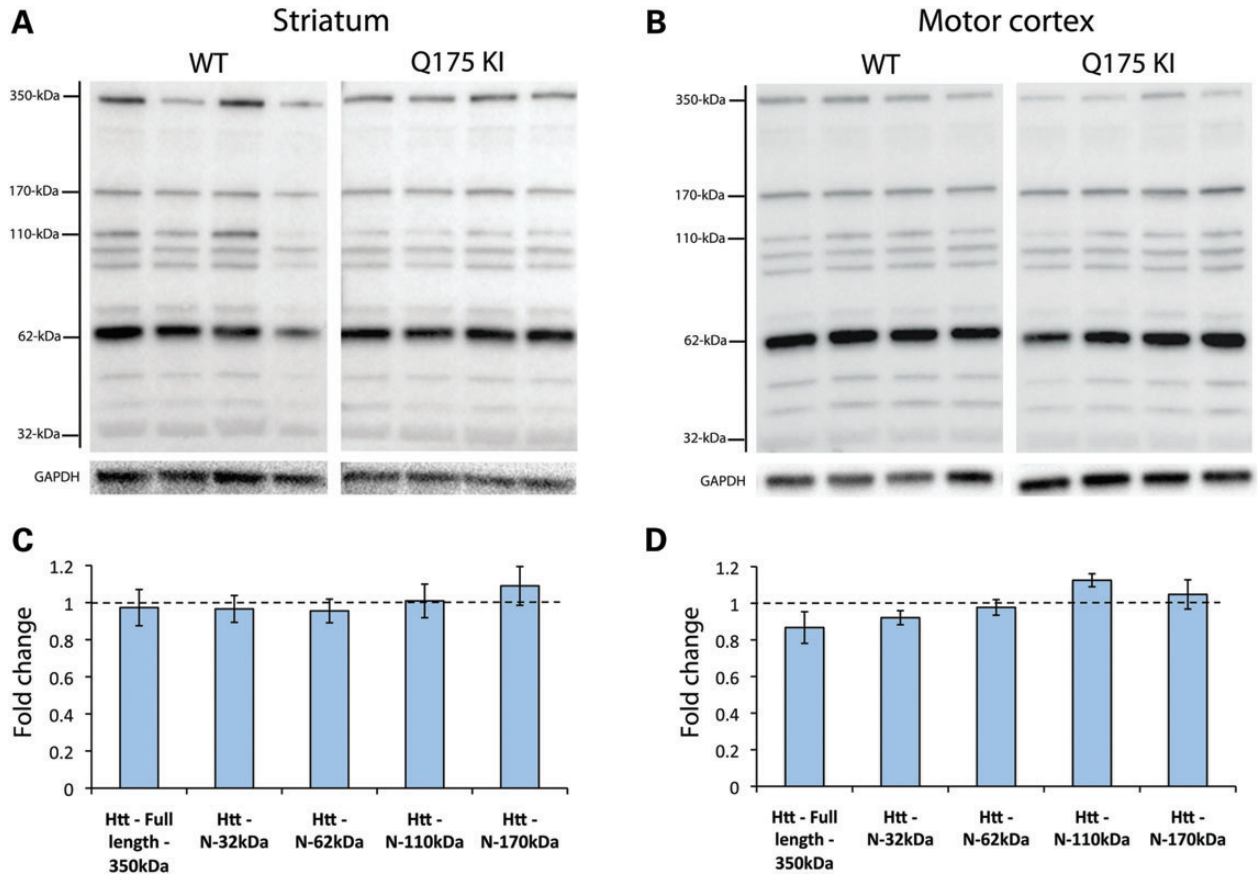

Figure 3. The protein levels of full-length huntingtin and N-terminal cleaved huntingtin fragments were assessed in heterozygous Q175 knock-in (Q175 KI) mice at 12 months of age. Western blots were performed using total lysate from the striatum (**A** and **B**) and motor cortex (**C** and **D**), using an antibody specific to the N-terminal region. Optical densities of the individual bands were quantified using NIH ImageJ and normalized to GAPDH on the same gel. Normalized optical densities of Q175 KI bands are expressed as fold change compared with the averaged value of normalized WT littermate control band densities, Mann–Whitney *U* tests. $N = 4–5$/group. Graphs are expressed as mean ± SEM.

Rab1A ($U = 1.00$, $P < 0.05$), respectively, in the prefrontal cortex of Q175 KI mice (Fig. 5E and F), yet these proteins did not change in other regions.

There were also numerous changes in the levels of pre- and post-synaptic proteins in the striatum, motor cortex, prefrontal cortex and hippocampus dissected from 12-month-old Q175 KI mice (Fig. 6). Presynaptic levels of the SNARE complex-associated protein SNAP-25 were decreased in the striatum ($U = 2.00$, $P < 0.05$) and hippocampus ($U = 2.00$, $P < 0.05$) (Fig. 6A, B, G and H). Synaptophysin, however, was increased in the hippocampus ($U = 1.00$, $P < 0.05$) of Q175 KI mice (Fig. 6G and H). Q175 KI mice also developed a reduction in the level of Rab3b ($U = 1.00$, $P < 0.05$) at 12 months of age in the motor cortex (Fig. 6C and D) and a reduction in Rab3A ($U = 2.00$, $P < 0.05$) in the hippocampus (Fig. 6G and H). Levels of the post-synaptic protein PSD-95 were decreased in the prefrontal cortex (Fig. 6E and F) yet remained unchanged in all other regions. A reduction in the protein levels of the glutamate receptors NMDAR1 ($U = 2.00$, $P < 0.05$) and NMDAR2 ($U = 2.00$, $P < 0.05$) was exclusively found in the hippocampus (Fig. 6G and H).

Axonal transport, cytoskeletal and synaptic changes were also investigated in 6-month-old Q175 KI mice (Supplementary Material, Figs S2 and S3), a time point where inclusions were more diffuse and no brain atrophy was observed. Proteins of interest were chosen based on those that were dysregulated in 12-month-old Q175 KI mice. At 6 months of age, protein levels of the retrograde transport motor protein dynein were decreased in the striatum of Q175 KI mice ($U = 0.00$, $P < 0.01$) compared with age-matched WT littermate controls (Supplementary Material, Fig. S2A and B), yet no changes in cytoskeletal and axonal proteins were found in the motor cortex (Supplementary Material, Fig. S2C and D). The mitochondrial trafficking protein Tom20 was decreased in the prefrontal cortex ($U = 2.00$, $P < 0.05$) of 6-month-old Q175 KI mice (Supplementary Material, Fig. S2E and F); however, there were no genotype-specific changes in transport protein levels in the hippocampus (Supplementary Material, Fig. S2G and H). There were specific reductions of presynaptic proteins in Q175 KI mice at 6 months of age. Although no changes in the SNARE complex-associated protein SNAP-25 were observed in the striatum in Q175 KI mice compared with age-matched WT littermates (Supplementary Material, Fig. S3A and E), the presynaptic associated GTPase Rab3b was decreased in the motor cortex ($U = 2.00$, $P < 0.05$) (Supplementary Material, Fig. S3B and F). Conversely, the post-synaptic density protein-95 (PSD-95) was not reduced in the PFC of Q175 KI mice at 6 months of age (Supplementary Material, Fig. S3C

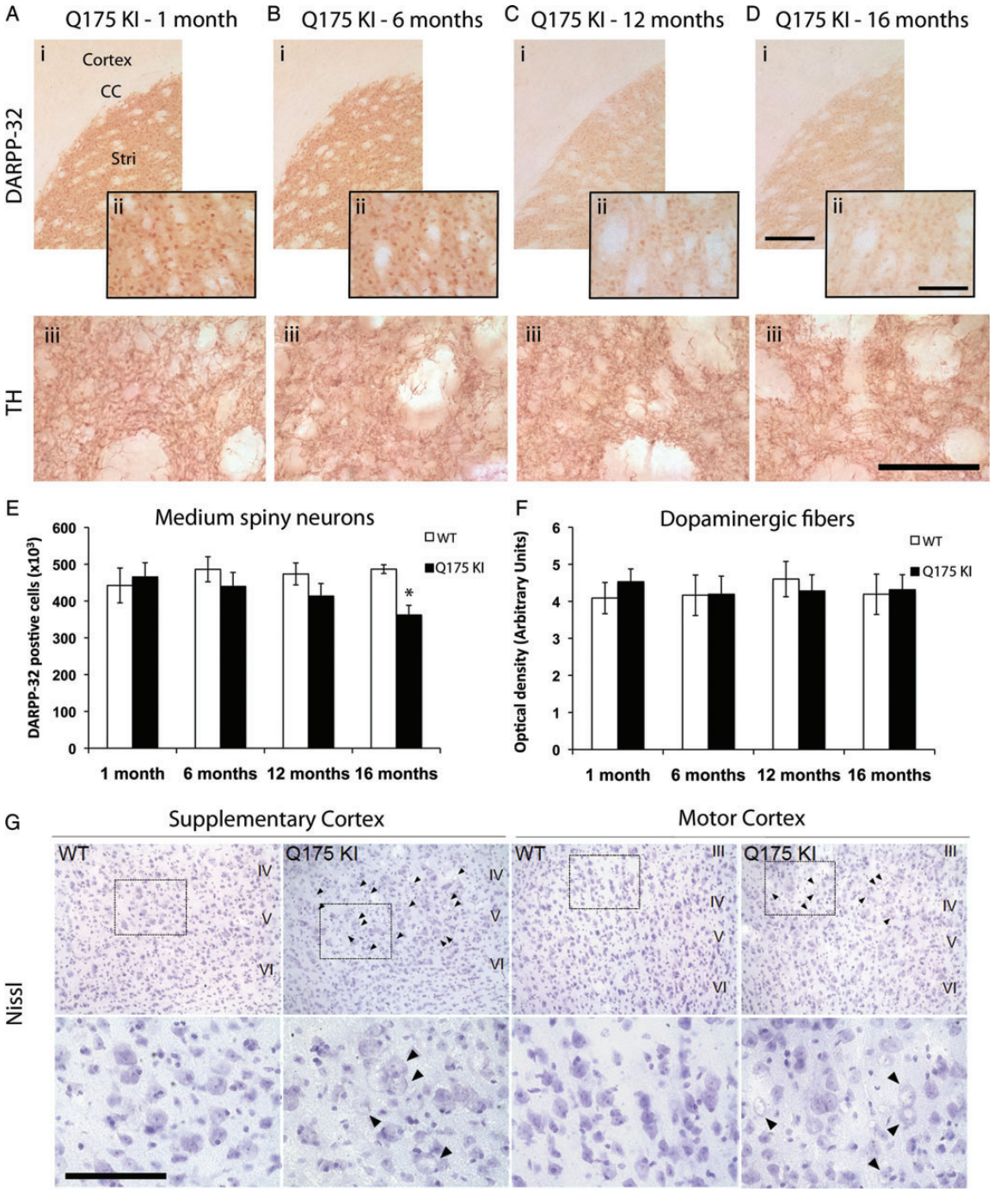

Figure 4. Histopathological findings in the striatum and cortex of heterozygous Q175 knock-in (Q175 KI) mice at 1, 6, 12 and 16 months of age. Immunolabeling for DARPP-32 and TH in Q175 KI mice shows the morphology of MSNs and dopaminergic fiber innervation in the striatum at 1, 6, 12 and 16 months of age (**A**i–**D**iii). Abbreviations: Stri, striatum and CC, corpus callosum. DARPP-32 protein levels decreased progressively with age (Ai–Dii), whereas TH-positive fibers remain unchanged (Aiii–Diii). Stereological analysis revealed that Q175 KI have a loss of MSN's at 16 months (**E**), yet there is no change in dopaminergic innervation as measured by optical density analysis (**F**). Nissl-stained sections from 12-month-old Q175 KI mice indicate swollen cell bodies and a loss of Nissl in the supplementary and motor cortex (**G**). Graphs are annotated as $^{*}P < 0.05$ compared with WT mice of the same age, two-way and MANOVAs with Dunnett's *post hoc* tests. $N = 8–12$/group. Graphs are expressed as mean ± SEM. Scale bars: Ai–Di = 250 μm, Aii–Dii = 100 μm, Aiii–Diii = 50 μm and G = 10 μm.

and G). In the hippocampus, both SNAP-25 ($U = 2.00$, $P < 0.01$) and Rab3A ($U = 1.00$, $P < 0.05$) protein levels were reduced, in contrast to synaptophysin protein levels that remained unchanged. The protein levels of glutamate receptors NMDAR1 and NMDAR2 also did not differ between genotypes at 6 months (Supplementary Material, Fig. S3D and H).

The majority of axonal transport, cytoskeletal and axonal transport changes present at 12 months were also found at the

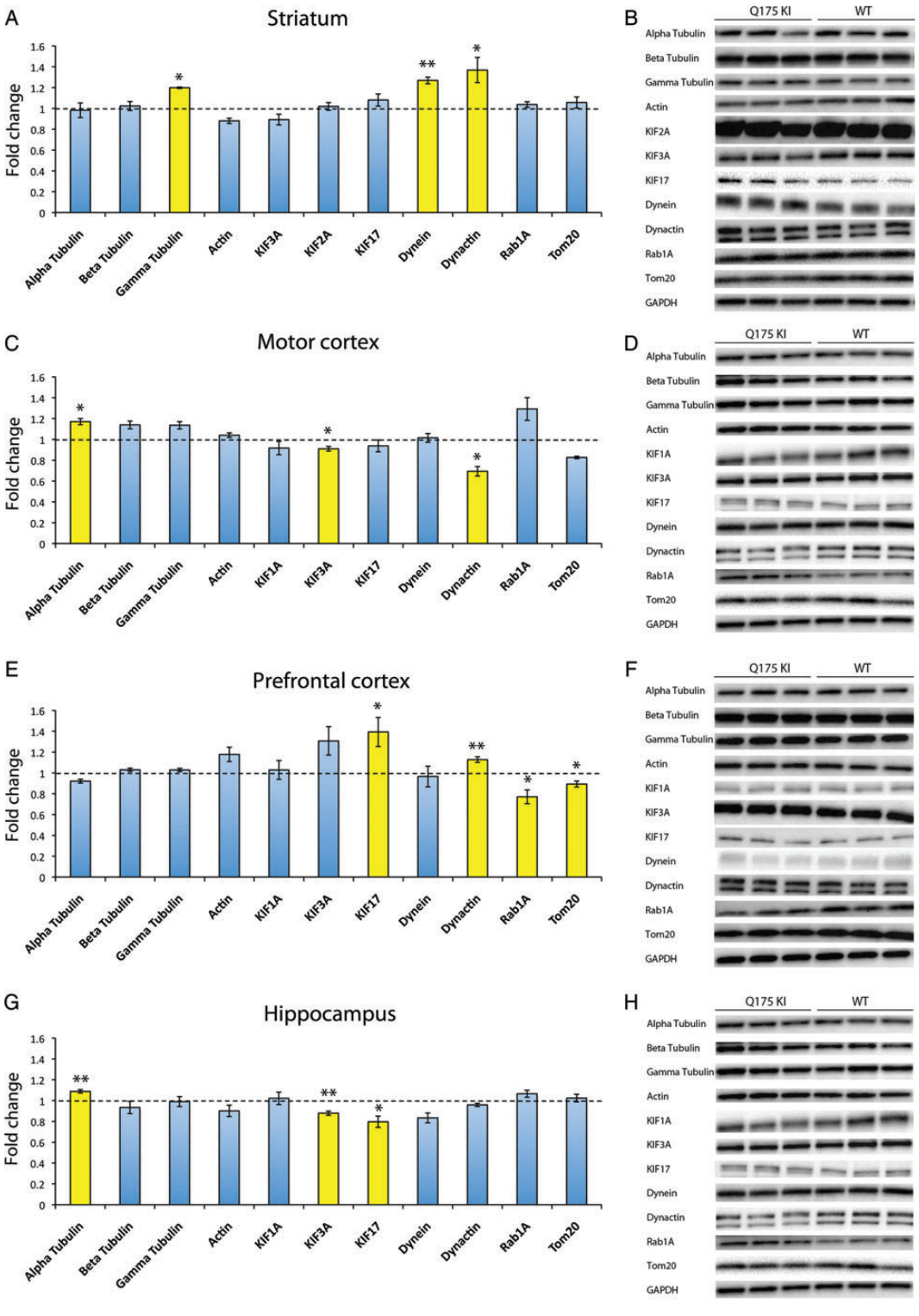

Figure 5. Cytoskeletal and axonal transport protein changes in heterozygous Q175 knock-in (Q175 KI) mice at 12 months of age. Western blots were performed using total lysate from the striatum (**A** and **B**), motor cortex (**C** and **D**), prefrontal cortex (**E** and **F**) and hippocampus (**G** and **H**) of Q175 KI mice and age-matched WT littermate mice. The cytoskeletal protein α-tubulin was increased in the motor cortex (C and D) and hippocampus (G and H), whereas γ-tubulin was increased in the striatum (A and B) of Q175 KI mice. Levels of the anterograde transport motor proteins KIF3A and KIF17 were decreased in the motor cortex (C and D) and hippocampus (G and H), yet KIF17 was increased in the prefrontal cortex (E and F). Levels of the retrograde transport motor proteins dynein and dynactin were increased in the striatum (A and B), whereas dynactin was increased in the prefrontal cortex (E and F). Conversely, dynactin was reduced in the motor cortex (C and D). The mitochondrial and Golgi to ER trafficking proteins, Tom20 and Rab1A, respectively, were decreased in the prefrontal cortex (E and F). Optical densities of the individual bands were quantified using NIH ImageJ and normalized to GAPDH on the same gel. Normalized optical densities of Q175 KI bands are expressed as fold change compared with the averaged value of normalized WT littermate control band densities and significance annotated as $^{*}P < 0.05$ and $^{**}P < 0.01$, Mann–Whitney U tests. $N = 5–8$/group. Graphs are expressed as mean ± SEM.

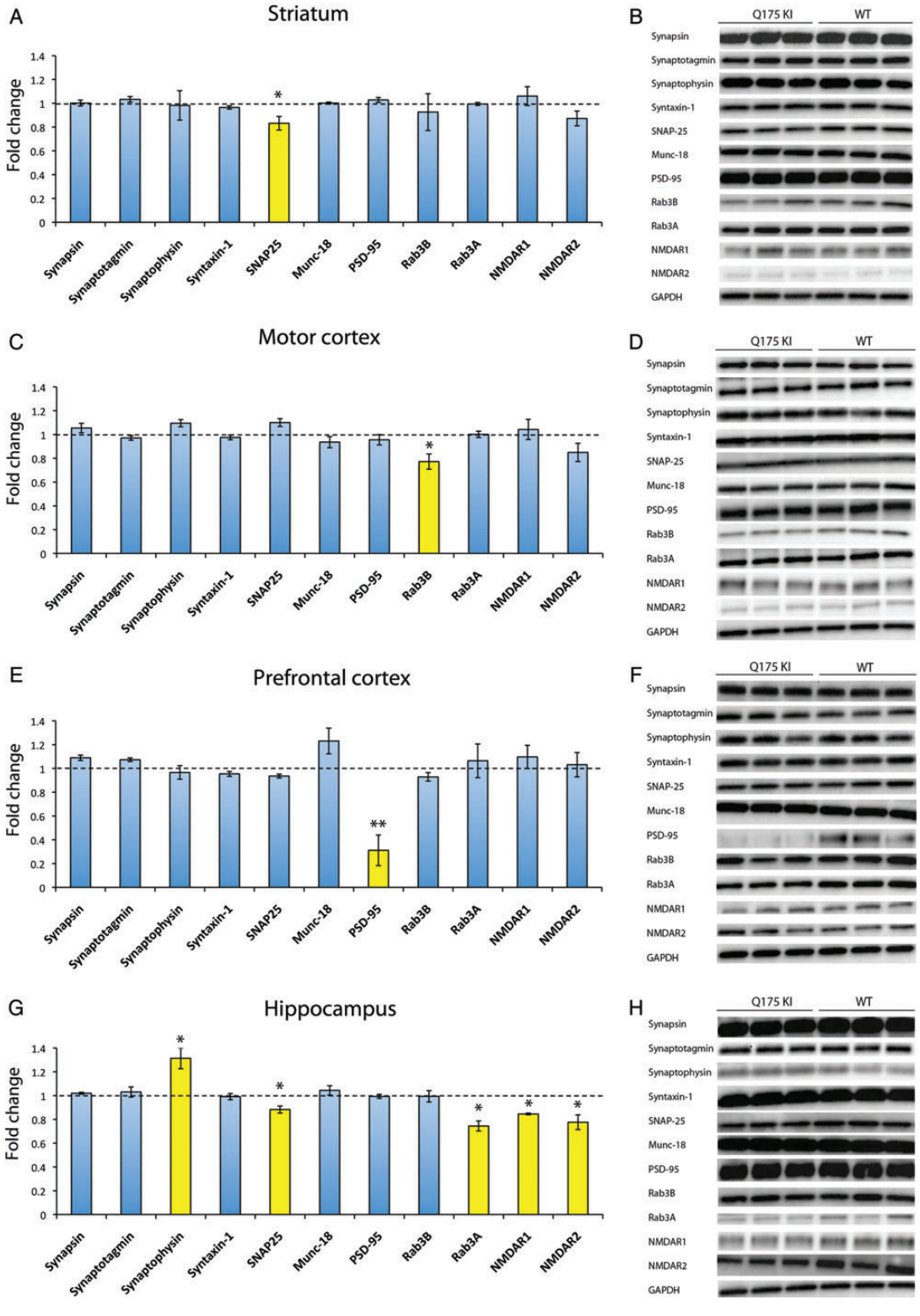

Figure 6. Synaptic protein changes in heterozygous Q175 knock-in (Q175 KI) mice at 12 months of age. Western blots were performed using total lysate from the striatum (**A** and **B**), motor cortex (**C** and **D**), prefrontal cortex (**E** and **F**) and hippocampus (**G** and **H**) of Q175 KI and age-matched WT littermate mice. Levels of the SNARE complex protein SNAP-25 was decreased in the striatum (A and B) and hippocampus (G and H), whereas synaptophysin was increased in the hippocampus (G and H) of Q175 KI mice. Levels of the presynaptic proteins Rab3b and Rab3A were decreased in the motor cortex (C and D) and hippocampus (G and H), respectively, whereas levels of the post-synaptic protein PSD-95 were decreased in the prefrontal cortex (E and F). NMDAR1 and NMDAR2 were also decreased in the hippocampus (G and H). Optical densities of the individual bands were quantified using NIH ImageJ and normalized to GAPDH on the same gel. Normalized optical densities of Q175 KI mouse bands are expressed as fold change compared with the averaged value of normalized WT littermate control band densities and significance annotated as $^{*}P < 0.05$ and $^{**}P < 0.01$, Mann–Whitney U tests. $N = 5–8$/group. Graphs are expressed as mean ± SEM.

16-month time point (Supplementary Material, Figs S4 and S5). Interestingly, synaptic proteins that were changed in 12-month-old Q175 KI mice were not different from WT levels at 16 months in the hippocampus region (Supplementary Material, Fig. S5G and H). There was no significant difference, as determined by Mann–Whitney *U* tests, in GAPDH protein levels between Q175 KI mice and WT mice at any age or region analyzed.

TrkB and BDNF protein level alterations in Q175 KI mice

Mutant Htt alters retrograde transport of TrkB receptors in striatal dendrites (32) and reduces the transport of BDNF from the cortex to the striatum. Loss of striatal BDNF was observed in HD brains at post-mortem (15,30). In Q175 KI mice that were 6 months of age, levels of TrkB ($U = 0.00$, $P < 0.01$) were decreased in the motor cortex, highlighting this as an early neurotrophic related change (Fig. 7A and B). At 12 months, the decrease in TrkB protein levels in the motor cortex persisted ($U = 1.00$, $P < 0.01$; Fig. 7C and D). There was no significant difference in GAPDH protein levels between Q175 KI mice and WT mice at any age or region analyzed. This increase in TrkB protein levels, seen at 12 months, was no longer present in 16-month-old Q175 KI mice (Fig. 7E and F). BDNF is also reduced in the *striata* of Q175 KI mice at 12 months of age ($F_{2,28} = 3.58$, $P < 0.05$), occurring when TrkB levels were elevated (Fig. 7H–G).

Neurotransmitter and metabolite level alterations in the striatum

Altered levels of neurotransmitters are detected throughout the basal ganglia of HD patients (15,30). We used high-performance liquid chromatography (HPLC) analysis to measure alterations of biogenic monoamines and amino acids in whole tissue homogenates of striatum from 1-, 6-, 12- and 16-month-old Q175 KI and WT mice (Table 2). An increase in the ratio of DOPAC/dopamine was detected in 6-month-old Q175 KI mice ($T_{1,13} = 2.22$, $P < 0.05$), which preceded reductions in striatal dopamine at 12 ($T_{1,14} = 5.01$, $P < 0.001$) and 16 months ($T_{1,14} = 2.24$, $P < 0.05$) of age. The decrease in dopamine was also paralleled by a reduction in the dopamine metabolite homovanillic acid (HVA) in Q175 KI mice at 12 ($T_{1,14} = 4.15$, $P < 0.001$) and 16 months ($T_{1,14} = 2.21$, $P < 0.05$). At 1 month of age, the striatal tissue content of GABA was increased in Q175KI mice ($T_{1,13} = 2.49$, $P < 0.05$) and remained elevated at 6 months ($T_{1,14} = 2.53$, $P < 0.05$) but was not different from age-matched WT levels at 12 and 16 months. Q175 KI mice also showed a decrease in the Glu/GABA ratio at 6 months ($T_{1,14} = 5.51$, $P < 0.001$) and 16 months ($T_{1,14} = 2.22$, $P < 0.05$). In contrast, there was no overall change in the levels of 5-HT in the striatum of Q175 KI mice at any age; however, at 12 months, a reduction in the 5-HT metabolite 5-HIAA was observed ($T_{1,14} = 2.92$, $P < 0.05$).

DISCUSSION

In summary, we show that the novel heterozygous Q175 KI mouse model of HD displays progressive behavioral, biochemical and neuropathological abnormalities that recapitulate changes seen in HD patients and their tissues at post-mortem. This heterozygous KI mouse model may therefore signify a more biologically meaningful model of HD compared with previously characterized Htt-overexpressing mice. In addition, we have demonstrated that levels of proteins involved in axonal transport, the cytoskeleton and synaptic transmission are altered before significant neuronal loss in Q175 KI mice. Such newly identified protein abnormalities are potentially critical to understanding deficits seen in HD, and methods to normalize these protein changes could be utilized in therapeutic paradigms.

Behavioral deficits and neuronal degeneration in Q175 KI mice

Q175 KI mice display progressive motor coordination deficits on the accelerating rotarod, which accompany the onset of mutant Htt inclusion formation, yet precede brain atrophy. Although deficits in motor coordination were observed in Q175 KI mice, observations of spontaneous motor behavior indicated that Q175 KI mice were also hyperactive. We found that hyperactivity and brain atrophy occurred simultaneously in the Q175 KI model at 12 months of age, in contrast to other transgenic rodent models where hyperactivity precedes cell death (48,49). At 12–16 months of age, Q175 KI mice also display motor, cognitive and motivational behavioral deficits, at which time striatal volume is reduced by 33% compared with WT mice, and motor cortex thickness is reduced by 18%. These degenerative changes are comparable with the human disease as a shrinkage of the caudate-putamen and motor cortex by 60 and 20%, respectively, has been observed in brains from late stage HD patients, compared with age-matched controls (50). HD patients display equal cell loss in cortical layers III, V and VI (51), which is most evident in the sensory-motor region (9). In Q175 KI mice, cortical layers III, IV and V contain swollen cell bodies, many of which show a dispersion of Nissl away from the center. These features occur during chromatolysis, which is associated with retrogradely degenerating neurons and often precedes apoptosis (52). Based on our behavioral and histopathological analyses, we find that the heterozygous Q175 KI mouse model of HD represents the most rapid heterozygous KI model to date (5,53), although it has a relatively slow phenotype compared with transgenic mutant Htt overexpression models of HD, such as R6/1 and R6/2 mice (44,54–56). The Q175 KI model, therefore, permits the examination of the early and progressive effects of full-length mutant Htt on a number of different systems also affected in human HD. Interestingly, a recent paper has shown an age-dependent deterioration of circadian rhythm in heterozygous Q175 KI mice (57), a symptom also observed in HD patients (58).

In mouse models of HD, the motor phenotype has been associated with altered striatal DA levels (49); however, dysregulation of striatal DA in HD patients is much less understood. It has been suggested that striatal DAergic signaling decreases at late stage (59), contributing to bradykinetic symptoms. Certainly, our data indicate that striatal DA levels are reduced at 12 and 16 months of age in Q175KI mice. In agreement, DA levels are reduced and its efflux impaired in both the YAC128 and the R6/2 mouse models at late stage (60). However, reduced dopamine levels may not be the only contributing factor to

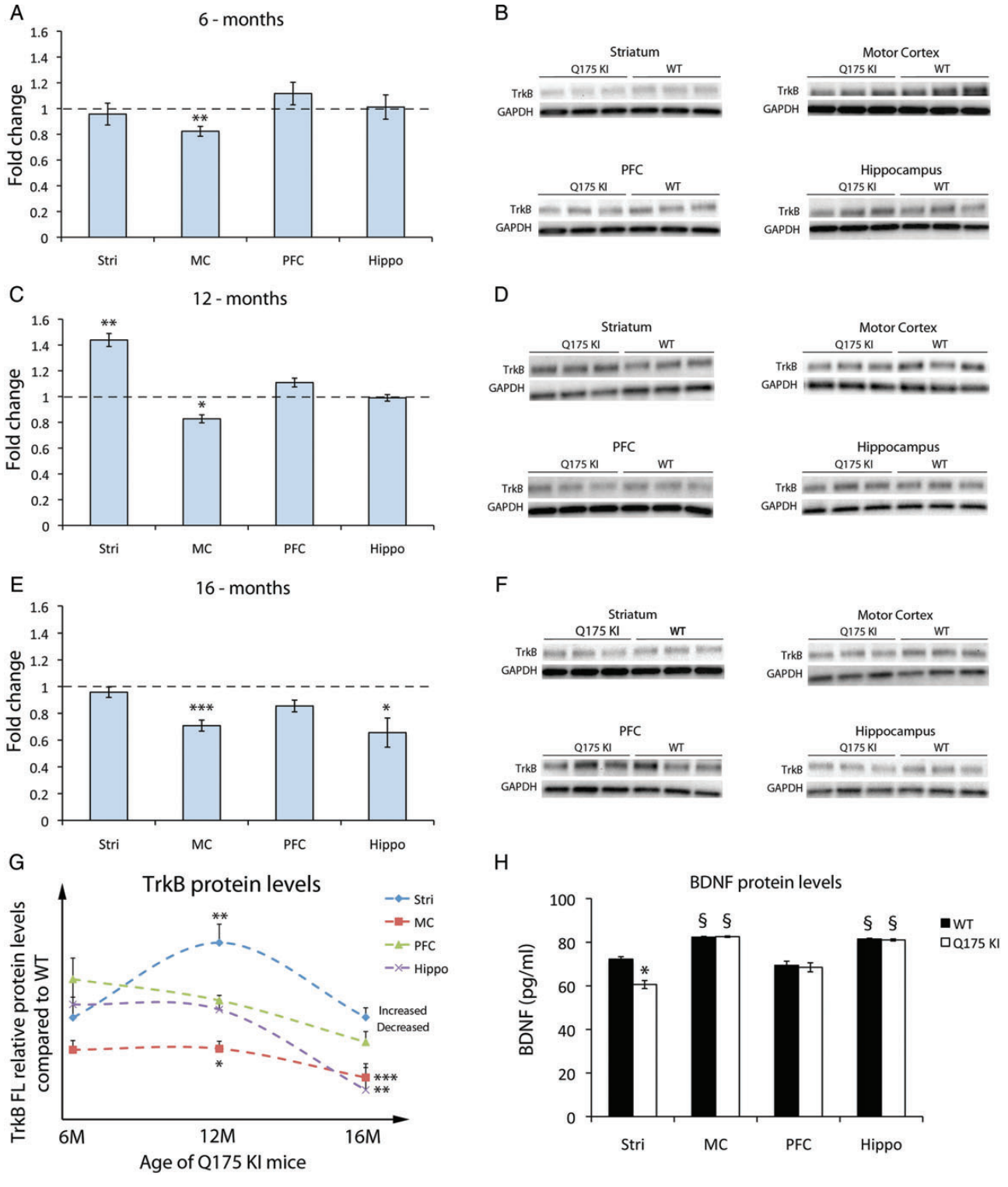

Figure 7. Brain-derived neurotrophic factor and neurotrophic tyrosine kinase receptor (TrkB) protein changes in heterozygous Q175 knock-in (Q175 KI) mice. Western blots were performed using total lysate from the striatum, motor cortex, prefrontal cortex and hippocampus of Q175 KI and age-matched WT littermate mice (**A**–**F**). Full-length TrkB was increased in the striatum of Q175 KI mice at 12 months (C and D), whereas TrkB was decreased in the motor cortex at 6, 12 and 16 months (A–F). There was also a reduction in full-length TrkB in the hippocampus at 16 months (E and F). A graphical representation of TrkB by region over time is also shown (**G**). Optical densities of the individual bands were quantified using NIH ImageJ and normalized to GAPDH on the same gel. Normalized optical densities of Q175 KI mouse bands are expressed as fold change compared with the averaged value of normalized WT littermate control band densities. In 12-month-old Q175 KI mice, BDNF levels were measured by ELISA (**H**) and were reduced in the striatum compared with WT littermate mice. Absorbency values per well were expressed as fold change compared with the averaged value of normalized WT littermate control absorbency values. Significance is annotated as $^{*}P < 0.05$ and $^{**}P < 0.01$, Mann–Whitney U tests. $N = 5$–8/group. Graphs are expressed as mean ± SEM.

Table 2. Age-dependent changes in neurotransmitter levels, ratios and metabolites in Q175 KI mice

Biochemical	1 month WT	1 month Q175 KI	6 months WT	6 months Q175 KI	12 months WT	12 months Q175 KI	16 months WT	16 months Q175 KI
DA	173.40 ± 8.17	178.90 ± 3.71	170.2 ± 7.08	161.1 ± 8.74	146.3 ± 2.73	**125 ± 0.05***** ↓	124.5 ± 2.83	**114.5 ± 5.15*** ↓
DOPAC	18.03 ± 0.62	18.76 ± 1.07	12.80 ± 0.58	14.71 ± 0.80	9.93 ± 0.44	**8.48 ± 0.47*** ↓	8.36 ± 0.34	**6.47 ± 0.66*** ↓
DOPAC/DA ratio	0.10 ± 0.00	0.10 ± 0.00	0.07 ± 0.00	**0.10 ± 0.01*** ↑	0.06 ± 0.00	0.07 ± 0.00	0.06 ± 0.00	0.06 ± 0.00
HVA	17.68 ± 1.02	17.93 ± 0.60	0.08 ± 0.00	0.08 ± 0.00	14.43 ± 0.76	**10.83 ± 0.00** * ↓	10.58 ± 0.69	**8.87 ± 0.24*** ↓
3-MT	18.60 ± 1.27	17.83 ± 1.27	13.80 ± 0.77	14.86 ± 1.56	14.22 ± 1.04	11.55 ± 1.37	12.37 ± 0.76	13.56 ± 0.76
5-HT	7.66 ± 0.47	8.495 ± 0.22	4.351 ± 0.20	4.945 ± 0.28	4.14 ± 0.15	3.82 ± 0.09	3.90 ± 0.22	4.17 ± 0.15
5-HIAA	4.14 ± 0.29	4.126 ± 0.16	3.481 ± 0.46	2.995 ± 0.28	3.81 ± 0.33	**2.74 ± 0.14*** ↓	2.92 ± 0.21	3.03 ± 0.28
Glu	37.42 ± 3.46	45.03 ± 2.43	32.96 ± 1.56	33.05 ± 1.94	30.18 ± 0.91	28.35 ± 0.71	19.48 ± 0.92	19.53 ± 0.65
GABA	5.94 ± 0.44	**7.390 ± 0.37***↑	5.509 ± 0.26	**6.985 ± 0.51*** ↑	6.29 ± 0.29	5.93 ± 0.25	4.35 ± 0.26	5.24 ± 0.41
Glu/GABA ratio	5.74 ± 0.18	6.090 ± 0.08	5.991 ± 0.07	**4.793 ± 0.20*** ↓	4.84 ± 0.20	4.81 ± 0.15	4.537 ± 0.20	**3.843 ± 0.23*** ↓

Units (ng/mg). Significantly altered neurotransmitter levels, ratios and metabolites seen in Q175 KI mice are indicated in bold and their relative change compared to WT is annotated by either an up or a down arrow.
WT, wild-type; Q175 KI, heterozygous Q175 knock-in mice; DA, dopamine; DOPAC, 3,4-dihydroxyphenylacetic acid; HVA, homovanillic acid; 3-MT, 3-methoxytyramine; 5-HT, 5-hydroxytryptamine; 5-HIAA, 5-hydroxyindoleacetic acid; Glu, glutamic acid and GABA, gamma-aminobutyric acid.
Significance annotated as $^{*}P < 0.05$, $^{**}P < 0.01$ and $^{***}P < 0.001$ by unpaired *T*-test compared with age-matched WT littermates and values as expressed as mean ± SEM. Arrows indicate direction of change compared with WT.

bradykinetic symptoms, as Q175 KI mice remain spontaneously hyperactive despite reduced DA levels. The change in the GABA/glutamate ratio seen in Q175 KI mice at late stage may be contributing to the observed hyperactivity through activation of MSNs in the direct pathway, by proportionally increased GABA compared with glutamate.

Mutant Htt inclusion formation in nuclear and perinuclear cellular compartments is considered a hallmark of HD progression in both humans (10) and mouse models (3,43–45). Q175 KI mice display mutant Htt inclusions at 6 months, which progressively increase in number with age. Inclusions were observed throughout the brain but were most dense in the striatum and cortex. Proteolytic cleavage of Htt is necessary for the targeting of N-terminal Htt fragments through the nuclear pores (61), where they may misfold owing to the polyglutamate repeat and become aggregate prone (62). Mouse models based on the expression of caspase-6 cleaved N-terminal Htt fragment display a rapid behavioral phenotype and brain atrophy (63). Thus, N-terminal Htt fragments are hypothesized to contribute to disease progression. We find that the relative protein levels of both full-length Htt and cleaved N-terminal Htt fragments do not differ between Q175 KI mice and WT mice. Therefore, our data do not support the hypothesis that Htt N-terminal fragment accumulation is responsible for the degenerative changes we find in the Q175 KI mouse model of HD.

Axonal transport and synaptic protein changes in Q175KI mice

Htt is a cytoplasmic protein associated with vesicle membranes and functions to control their anterograde and retrograde transport on microtubules (18–21). Normal axonal transport of synaptic proteins from the ER to the terminals is also essential for maintaining dendritic spines and synapses (17). Mutant Htt interferes with axonal transport through both vesicle motility-associated protein interactions and physically after aggregation (22–26); however, key transport and synaptic protein level changes that occur during this process remain poorly understood. Our data revealed that several proteins involved in retrograde and anterograde axonal transport were altered in Q175 KI mice, including kinesins, dynein and dynactin. An increase in striatal dynein levels was first observed at 6 months of age, at which time an accumulation of aggregated mutant Htt is apparent but neurodegeneration, as reflected by striatal atrophy or cortical thinning, is not yet observed. Altered levels of axonal transport proteins persist in 12-month-old Q175 KI mice, when there is both widespread mutant Htt aggregation and atrophy of the cortex and striatum. Our data showing increased levels of the retrograde transport protein dynactin in the striatum, in parallel with its reduction in the motor cortex, suggest that retrograde transport may be reduced in the corticostriatal pathway in Q175 KI mice at 6 and 12 months of age. Disruption of retrograde transport perturbs numerous cellular processes, including mutant Htt protein clearance by the lysosome and proteosome (64) and mitochondrial degradation in the autophagosome (65,66). Protein levels of dynein have not yet been studied in HD patient's brains, yet this protein may be of importance for future investigation given *in vitro* findings showing loss of binding to microtubules (27,28) and its implication in other neurodegenerative diseases, reviewed in (67). Kinesin-driven anterograde transport from the cortex is essential to supply BDNF to the striatum (68,69), and we observed reduced KIF3A levels in the motor cortex of Q175KI mice.

Striatal BDNF levels were reduced in 12-month-old Q175 KI mice, in agreement with findings in other HD mouse models (32,70,71) and HD patients (15,31). Levels of the BDNF receptor, TrkB, were increased in the striatum at the same time point, possibly indicating a compensatory response to striatal BDNF depletion. This increase was not observed at 16 months, suggesting that this system modification is transient. Conversely, TrkB levels were decreased in the motor cortex at 12 and 16 months. It is therefore reasonable that at longer time points, TrkB would be decreased in both the motor cortex and striatum of Q175 KI mice, likely the result of the transcriptional repression of BDNF (31), which may occur secondary to vesicle motility problems. BDNF depletion causes reduced signaling through mitogen-activated protein kinases 1 and 2 and extracellular signal-regulated kinase (72), which are required for normal synaptic

plasticity (73). Ameliorating striatal BDNF loss in the striatum therefore remains a viable neuroprotective strategy in HD that could be tested in the Q175 KI mouse model of HD.

Mutant Htt also causes progressive synaptic dysfunction and dendritic spine instability in HD mouse models (74,75), and in HD patients, synaptic deficits occur at early disease stages (76). Synaptic plasticity, in the form of long-term potentiation (LTP), has been found to be impaired in the cortex, striatum and hippocampus of HD patients (12) and HD mouse models (13,38–42). Q175 KI mice also show reduced tonic inhibition in striatal output neurons by loss of astrocytic GABA release (77). Similarly, Q175 KI mice display a reduction in EPSC's of MSNs, after cortical stimulation, at 6 months of age (78). Our data suggest that synaptic abnormalities may be part-mediated by small Rab GTPases, which function at the synapse and influence vesicle release. Rab3A is fundamental for LTP in the hippocampus (79), and the decrease in Rab3A protein expression in the hippocampus of the Q175 KI model may also influence memory deficits. Rab3A is also reduced in HD brains at post-mortem (80). We also find that Rab3b is reduced in the motor cortex region at 6–16 months and suggest this may underlie electrophysiological changes that occur at the same age (78).

We also show that mutant Htt has detrimental effects on the levels of both pre- and post-synaptic proteins, which may be responsible for such electrophysiological signatures. Levels of the presynaptic SNARE complex protein SNAP-25 were reduced in the striatum of Q175 KI mice (<30%). Reductions to a similar extent have also been reported in grade 1 HD patient's brains at post-mortem (80). In contrast, levels of the post-synaptic protein, PSD-95, were reduced (<70%) in the PFC region of the Q175 KI mice, yet have not been evaluated in HD patient brain tissue. Both SNAP-25 and PSD-95 are modulated by Htt interacting protein-14 (HIP-14) (81) and therefore reduced associations between mutant Htt and HIP-14 may underlie the loss of these proteins. It is important to note that the relatively small magnitude of several of the protein changes detected in the current study may reflect a dilution effect caused by assessing changes in total homogenate samples by western blot and the detection thresholds achievable by the technique. In fact, the extent of changes in specific populations of cells may have been underestimated owing to the presence of noncontributing cells contained within the same sample. Nonetheless, as discussed earlier, protein changes of similar sizes have been previously documented by western blot analysis of HD patient brains at post-mortem (80), thereby validating the Q175 KI mouse as a realistic model of the human disease.

CONCLUSIONS

Given the loss-of-function phenotypes associated with Htt knockdown (1), reviewed in (82), it is important to model the clinically common heterozygous condition in heterozygous KI mice. The Q175 KI mouse model provides a biologically meaningful model of human HD and avoids possible overexpression artifacts that might be observed when analyzing transgenic HD mouse models. Our data provide evidence of early pre-degenerative changes and late stage brain atrophy in Q175 KI mice, with HD patient-like heterozygosity of mutant and WT Htt expression, and such changes were reflected in motor and cognitive behavioral abnormalities. Therapeutic interventions designed to modulate abnormalities in specific axonal transport and synaptic proteins found in this study may reduce disease progression and are therefore an area of future investigation.

MATERIALS AND METHODS

Mice

Heterozygous Q175 knock-in (Q175 KI) mice on the C57Bl/6 background and WT littermate controls were purchased from Jackson Laboratories. The CAG repeat sequence of each Q175 KI cohort was assessed to be in the range of 173 to 190. Mice arrived in three cohorts of different ages: 1 month ($N = 48$), 6 months ($N = 48$) and 12 months ($N = 119$). A proportion of the 12-month cohort was aged in-house until 16 months of age ($N = 25$). At each time point, mice were assessed for behavioral deficits and were sacrificed for histology, western blot or biochemical analysis. Until sacrifice, mice were housed in standard conditions in a dark/light cycle of 12 h, with *ad libetum* access to food and water. All animal procedures were performed in accordance with National Institute of Health guidelines and were approved by the Institutional Animal Care and Use Committee at McLean Hospital, Harvard Medical School.

Spontaneous activity in a cylinder

Mice were placed in cylinders of 15 cm in height and 12 cm in diameter to freely explore for 3 min. Mirrors were placed directly behind and underneath the cylinder such that spontaneous movements in any direction were recorded by the video camera (Sony HDR–CX160). Each video was analyzed on i-movie (119.0.4), by an investigator blind to the experimental groups. Videos were scored in slow motion allowing the investigator to record the following: (i) total forepaw steps on the base of the cylinder, (ii) total hindpaw steps on the base of the cylinder, (iii) total number of rears and (iv) time spent grooming.

Rotarod

Mice were placed on a 5-cm division of the rotating beam in the rotarod (Ugo Basile, 47600 V04), set to rotate in an accelerating protocol of 3–44 rpm over 3 min. The latency to fall was automatically logged by the mouse tripping a time switch upon landing on the base of the equipment, and times were recorded in an investigator blind fashion. Mice performed the test five times with intervals of 15 min or more, and the scores from runs 2–5 were averaged for each mouse.

Y-maze

The Y-maze tests spontaneous alternation behavior, which is regarded as a measure of working memory, previously defined by Hu *et al.*, (83). The Y-maze consists of three arms set at equal angles (labeled A, B and C). Specific dimensions of each arm are H: 37 cm, W: 9 cm and D: 10 cm. 16-month-old Q175 KI mice and age-matched WT littermates were tested once in the Y-maze investigator blind paradigm. Each mouse was placed at the end of arm A and allowed to move freely through the maze during an 8-min session. The sequence and number

of arm entries were recorded manually. Spontaneous alternation was defined as entries into all three arms on consecutive occasions (i.e. ACB, ABC, BCA and CBA), rather than reentry into a corridor visited previously (i.e. ACC, ABB, AAC, AAB and AAA). The percentage alternation was calculated as the ratio of actual to possible alternations (the total number of arm entries -2×100).

Nest scoring

Nesting is goal-directed behavior, controlled by levels of arousal and motivation (i.e. the need for comfort and warmth). 16-month-old Q175 KI mice and age-matched WT littermates were singly housed with a 5 × 5 cm square of cotton bedding (Ancare) placed directly in the center. Mice were left uninterrupted for 16 h in 5 p.m.–9 a.m., and the nests were scored in an investigator blind fashion after the elapsed time. Scoring was conducted according to Deacon (84). The scoring system in brief was: 0 = uninterrupted nesting material, 1 = disturbed nesting material, 2 = flat nest of a saucer-like shape, 3 = moderate nest of a cup-like shape, 4 = incomplete dome and 5 = complete dome. After the initial score, a further deduction of either 0.25, 0.5 or 0.75 was implicated if each of the four nest walls fell below the initial scoring category.

Histology

At the end of behavioral testing, mice were terminally anesthetized with sodium pentobarbital and perfused transcardially with 25 ml of heparinized saline (0.1%) followed by 100 ml of 4% paraformaldehyde in phosphate buffer. Brains were removed and post-fixed in 4% paraformaldehyde for 4 h before placing them 25% sucrose. Coronal sections were cut to 40 μm, on a freezing sledge microtome and stored in antifreeze at −20°C until use. For immunohistochemistry, sections were rinsed in PBS before endogenous peroxidases were quenched in 3% hydrogen peroxide for 7 min. After rinsing, the sections were incubated in 5% normal goat serum in 0.1% Triton X-100 in PBS. Tissue sections were then incubated with either anti-Huntingtin (Chemicon, 1:1000), anti-DARRP-32 (Cell Signaling 1:1000), anti-NeuN (Millipore, 1:1000) or anti-TH (PelFreez 1:500). After washing in PBS, sections were incubated in biotinylated secondary antibody (anti-mouse/rabbit raised in goat at a concentration of 1:200). Staining of the tissue-bound antibody was visualized using a standard peroxidase-based method using an ABC kit (Vectastain Elite, Vector Laboratories, Burlingame CA, USA) and chromogen, 3,3′-diaminobenzadine (DAB, Sigma). For Nissl staining, tissue sections were mounted onto slides, dried and then hydrated in 70% ethanol, 50% ethanol and distilled water before exposure to 0.5% Cresyl violet for 4 min. Cresyl violet staining was differentiated in 95% ethanol and acetic acid (0.5 ml/200 ml). After staining, all tissue sections were dehydrated and coverslipped.

Immunoblotting

Mice were terminally anesthetized and perfused transcardially with heparinized saline (0.1% heparin in 0.9% saline), and brains were cut with the use of a tissue chopper at 750 μm. Tissue samples were collected from the striatum, motor cortex, prefrontal cortex and hippocampus of 6-, 12- and 16-month-old Q175 KI and age-matched WT littermate mice and each suspended in ice cold buffer containing: 300 mM sucrose in TE buffer (Bio-Rad). Phosphatase inhibitors I and II (1:100), proteinase inhibitors (1:100) (Thermo Halt proteinase inhibitor single use cocktail) and EDTA were then added. Tissues were homogenized for 15 s and sonicated in with three short pulses. A portion of the supernatant was reserved for protein determination (BCA Assay, Pierce), and the remaining solution was stored at −20°C. 15–30 mg of proteins from tissue preparations were then used to run each gel. Samples were loaded into the Criterion precast 4–12.5% SDS–polyacrylamide gel system (Bio-Rad). The proteins were then transferred from the gel to a PVDF membrane electrically charged at 21 V and 2.5 amps for 7 min. Membranes were washed in Tris-buffered saline with 0.1% Tween 20 (TBS-T). After at least 1 h of blocking in 5% blocker (Bio-Rad), the membranes were incubated overnight at 4°C in the following primary antibodies: α-tubulin (Upstate, 1:5000), β-tubulin (Chemicon, 1:5000) γ-tubulin (Sigma, 1:5000), Actin (Sigma, 1:1000), KIF3A (Abcam, 1:1000), KIF2A (Abcam, 1:5000), KIF17 (Abcam, 1:500), dynein (Santa Cruz, 1:250), dynactin (Santa Cruz, 1:1000), Rabphillin1A (ProteinTech, 1:1000), Tom-20 (Santa Cruz, 1:1000), synapsin (Thermo, 1:1000), synaptotagmin (BD Trans, 1:5000), synaptophysin (Santa Cruz, 1:500), syntaxin-1 (Millipore, 1:2000), SNAP-25 (Chemicon, 1:4000), Munc-18 (Thermo, 1:3000), PSD-95 (NeuroMab, 1:250), Rabphillin3B (ProteinTech, 1:1000), Rabphillin3A (BD Trans, 1:1000), NMDAR1 (BD Trans, 1:1000), NMDAR2 (Millipore, 1:1000), TrkB (Cell signaling, 1:200) and GAPDH (Millipore, 1:5000). After washing in TBS-T, HRP-conjugated secondary antibodies were then applied for 1 h at room temperature. The blots were treated with ECL-Plus (Amersham Biosciences) and exposed using ChemiDoc™ XRS and image Lab™ software. Optical density analysis (NIH image) was used to determine the relative abundance of each protein of interest. Bands were normalized to GAPDH for that same sample and gel, and Q175 KI band intensities were expressed as fold change compared with the average of the normalized WT bands. GAPDH levels were also directly compared between Q175 KI and WT mice, using optical density analysis of exposed bands, to ensure the adequate protein loading of the samples and to indicate that mutant Htt did not affect levels of GAPDH in any brain region or age analyzed.

BDNF ELISA

Striatal, PFC, MC and hippocampal tissue samples from 12-month-old Q175 KI mice and WT littermate controls were dissected and processed for use with mouse BDNF ELISA Kit (Syd Labs). Homogenates were prepared in PBS containing a proteinase inhibitor cocktail (Thermo). A portion of the supernatant was reserved for protein determination (BCA Assay, Pierce), and the remaining solution was stored at −20°C. The protocol was standardized for detection of low target protein concentrations (31.2–2000 pg/ml). 0.1 ml of each sample was added to each well and incubated at 37°C for 90 min. The plate contents were discarded and 0.1 ml of the anti-mouse BDNF antibody working solution added to each well. This was left to incubate at 37°C for 60 min. After three washes in 0.01 M TBS, the provided ABC solutions were incubated in wells

at 37°C for 60 min. After the final washes in TBS, the TMB color-developing solution was added and left to incubate at 37°C in the dark for 30 min, before the color reaction stop solution was added. Optical density absorbance at 450 nm was then read on a microplate reader. Absorbance levels were compared with a standard curve plotted from provided standards in the kit and was calculated as (the relative OD_{450}) = (the average OD_{450} of a sample triplicate) − (the average OD_{450} of the TBS only triplicate).

Biochemical analysis of neurotransmitters and metabolites

Mice were terminally anesthetized and perfused transcardially with heparinized saline (0.1% heparin in 0.9% saline). Whole brains were cut by a tissue chopper in 750-μm slices, and the striatum was dissected from two adjacent sections on ice. Tissue pieces were sent to CMN/KC Neurochemistry Core Laboratory in Vanderbilt University for HPLC analysis as defined in Chung *et al*. (6). In brief, the brain sections were homogenized in 200–750 μl of 0.1 M TCA, $10-4$ M EDTA and 10.5% methanol with $10-2$ M sodium acetate, using a tissue dismembrator (Fisher Scientific) and spun at 10 000 g for 20 min. The supernatant was removed and stored at −80°C. Neurotransmitters and metabolites present in the supernatant were determined by a specific HPLC assay using an Antec Decade II (oxidation: 0.5) electrochemical detector operated at 33°C. Twenty microliters of samples of the supernatant were injected onto a Phenomenex Nucleosil (100A) C18 HPLC column using a Water 717+ autosampler. The solvent was delivered at 0.8 ml/min using a Waters 515 HPLC pump. Using this solvent, the following biogenic amines evaluated: dopamine, DOPAC, HVA, 3-MT, 5-HIAA, 5-HT, GABA and glutamate. Waters Empower software was used for both controlling HPLC parameters during data collection and for data analysis.

Semi-quantitative scores for huntingtin inclusions

Semi-quantitative scores for the appearance of mutant Htt inclusions throughout the Q175 KI mouse brains were performed according to Bayram-Weston *et al*. (3). Scores in brief are: --, absent; *, weak nuclear staining; **, diffuse nuclear staining; ***, few inclusions and ****, many dense inclusions. Inclusions were analyzed in the following regions: striatum (lateral, medial, rostral and caudal quadrants), nucleus accumbens, septum, amygdala, thalamus, hypothalamus, hippocampus, motor cortex, prefrontal cortex, sensory cortex, piriform cortex and *s. nigra*. Htt inclusion appearance was confirmed for each region and age using five serial sections ($N = 6$ mice/group). Negative staining of inclusions was also confirmed at each age in WT mice.

Thickness, volumetric, cell number and densitometry measurements

Estimates of striatal volume and cortical thickness were defined on Nissl-stained sections using Stereo Investigator (MBF Bioscience), by an investigator bind to the genotypes. Striatal volume was determined by drawing contours around the striatum on each section, and the estimate was determined using the Optical Fractionater Workflow function. Parameters: number of sections (9–11/mouse), section evaluation interval 6 and the measured section thickness (~19–24 μm/section) at 10× magnification. Stereological estimates of DARPP-32 and NeuN cell numbers in the striatum and CA1/CA3 hippocampus regions, respectively, were counted using the same parameters at 20× magnification. The thickness of the PFC and motor cortex were measured using the Quick measure line tool from the upper most part of the cortex down to the cingulum. Sections were chosen for the PFC at approximately +2.58 mm and for the motor cortex at +1.18 mm relative to Bregma.

Optical density analysis of DARPP-32-stained tissue sections was performed using image J software (Version 1.46r). Striatal images were taken at 2.5× magnification, approximately +0.8 mm relative to bregma in the anterior–posterior direction. This microscopy was performed using a Zeiss Axioskop microscope, and images were taken with the Spot RT color camera (Diagnostic instruments, Inc.) using Spot software (Version 4.1.1). Photomicrographs were duplicated, converted to gray scale and inverted. Optical density values were then obtained for each image using the line tool to draw a contour around the striatum (excluding the nucleus accumbens) followed by the measure function. Optical density values were first normalized to background levels, by subtracting values of the corpus callosum. The level of DARPP-32 was calculated as the % difference of Q175 KI mouse levels at 1, 6, 12 and 16 months compared with the mean of age-matched WT mouse levels.

Statistical analysis

The Shapiro–Wilk test of normality was first conducted on all data sets to determine the sample distribution, using IBM© SPSS version 20. Data sets with significance above the alpha level of 0.05 was considered normally distributed and standard parametric tests employed. Unpaired student's *t*-test analysis was used to compare WT and heterozygous Q175 KI mice on a single dependent measure. When comparing two means for skewed data sets, the non-parametric Mann–Whitney *U* test was conducted. Two-way ANOVA and multivariate ANOVA (MANOVA) with Bonferroni *post hoc* tests were also used to compare both genotypes in all time points. All parametric and non-parametric test analyses were conducted using GraphPad Prism (Version 5.0) (GraphPad Software, Inc.). Statistical significance was determined at the alpha level of 0.05.

SUPPLEMENTARY MATERIAL

Supplementary Material is available at *HMG* online.

ACKNOWLEDGEMENTS

We thank Theresa Brand, Aarthi Subramanian, Jon Beagan and Sayantan Deb for their excellent technical assistance.

Conflict of Interest statement. None declared.

FUNDING

This project was funded by Cure Huntington's Disease Initiative Foundation (CHDI) (OI) and generous contributions from the Vaughan family (OI).

REFERENCES

1. Dragatsis, I., Levine, M.S. and Zeitlin, S. (2000) Inactivation of Hdh in the brain and testis results in progressive neurodegeneration and sterility in mice. *Nat. Genet.*, **26**, 300–306.
2. Bayram-Weston, Z., Jones, L., Dunnett, S.B. and Brooks, S.P. (2012) Light and electron microscopic characterization of the evolution of cellular pathology in HdhQ92 Huntington's disease knock-in mice. *Brain Res. Bull.*, **88**, 171–181.
3. Bayram-Weston, Z., Torres, E.M., Jones, L., Dunnett, S.B. and Brooks, S.P. (2012) Light and electron microscopic characterization of the evolution of cellular pathology in the Hdh(CAG)150 Huntington's disease knock-in mouse. *Brain Res. Bull.*, **88**, 189–198.
4. Woodman, B., Butler, R., Landles, C., Lupton, M.K., Tse, J., Hockly, E., Moffitt, H., Sathasivam, K. and Bates, G.P. (2007) The Hdh(Q150/Q150) knock-in mouse model of HD and the R6/2 exon 1 model develop comparable and widespread molecular phenotypes. *Brain Res. Bull.*, **72**, 83–97.
5. Menalled, L., El-Khodor, B.F., Patry, M., Suarez-Farinas, M., Orenstein, S.J., Zahasky, B., Leahy, C., Wheeler, V., Yang, X.W., MacDonald, M. *et al.* (2009) Systematic behavioral evaluation of Huntington's disease transgenic and knock-in mouse models. *Neurobiol. Dis.*, **35**, 319–336.
6. Chung, C.Y., Koprich, J.B., Siddiqi, H. and Isacson, O. (2009) Dynamic changes in presynaptic and axonal transport proteins combined with striatal neuroinflammation precede dopaminergic neuronal loss in a rat model of AAV alpha-synucleinopathy. *J. Neurosci.*, **29**, 3365–3373.
7. Vonsattel, J.P., Myers, R.H., Stevens, T.J., Ferrante, R.J., Bird, E.D. and Richardson, E.P. Jr (1985) Neuropathological classification of Huntington's disease. *J. Neuropathol. Exp. Neurol.*, **44**, 559–577.
8. Macdonald, V. and Halliday, G. (2002) Pyramidal cell loss in motor cortices in Huntington's disease. *Neurobiol. Dis.*, **10**, 378–386.
9. Rosas, H.D., Liu, A.K., Hersch, S., Glessner, M., Ferrante, R.J., Salat, D.H., van der Kouwe, A., Jenkins, B.G., Dale, A.M. and Fischl, B. (2002) Regional and progressive thinning of the cortical ribbon in Huntington's disease. *Neurology*, **58**, 695–701.
10. Sapp, E., Penney, J., Young, A., Aronin, N., Vonsattel, J.P. and DiFiglia, M. (1999) Axonal transport of N-terminal huntingtin suggests early pathology of corticostriatal projections in Huntington disease. *J. Neuropathol. Exp. Neurol.*, **58**, 165–173.
11. Zheng, Z. and Diamond, M.I. (2012) Huntington disease and the huntingtin protein. *Prog. Mol. Biol. Transl. Sci.*, **107**, 189–214.
12. Crupi, D., Ghilardi, M.F., Mosiello, C., Di Rocco, A., Quartarone, A. and Battaglia, F. (2008) Cortical and brainstem LTP-like plasticity in Huntington's disease. *Brain Res. Bull.*, **75**, 107–114.
13. Cummings, D.M., Milnerwood, A.J., Dallerac, G.M., Vatsavayai, S.C., Hirst, M.C. and Murphy, K.P. (2007) Abnormal cortical synaptic plasticity in a mouse model of Huntington's disease. *Brain Res. Bull.*, **72**, 103–107.
14. Seo, H., Sonntag, K.C. and Isacson, O. (2004) Generalized brain and skin proteasome inhibition in Huntington's disease. *Ann. Neurol.*, **56**, 319–328.
15. Zuccato, C., Marullo, M., Vitali, B., Tarditi, A., Mariotti, C., Valenza, M., Lahiri, N., Wild, E.J., Sassone, J., Ciammola, A. *et al.* (2011) Brain-derived neurotrophic factor in patients with Huntington's disease. *PLoS One*, **6**, e22966.
16. Millecamps, S. and Julien, J.P. (2013) Axonal transport deficits and neurodegenerative diseases. *Nat. Rev. Neurosci.*, **14**, 161–176.
17. Richards, P., Didszun, C., Campesan, S., Simpson, A., Horley, B., Young, K.W., Glynn, P., Cain, K., Kyriacou, C.P., Giorgini, F. *et al.* (2011) Dendritic spine loss and neurodegeneration is rescued by Rab11 in models of Huntington's disease. *Cell Death Differ.*, **18**, 191–200.
18. Hoffner, G., Kahlem, P. and Djian, P. (2002) Perinuclear localization of huntingtin as a consequence of its binding to microtubules through an interaction with beta-tubulin: relevance to Huntington's disease. *J. Cell. Sci.*, **115**, 941–948.
19. DiFiglia, M., Sapp, E., Chase, K., Schwarz, C., Meloni, A., Young, C., Martin, E., Vonsattel, J.P., Carraway, R., Reeves, S.A. *et al.* (1995) Huntingtin is a cytoplasmic protein associated with vesicles in human and rat brain neurons. *Neuron*, **14**, 1075–1081.
20. Velier, J., Kim, M., Schwarz, C., Kim, T.W., Sapp, E., Chase, K., Aronin, N. and DiFiglia, M. (1998) Wild-type and mutant huntingtins function in vesicle trafficking in the secretory and endocytic pathways. *Exp. Neurol.*, **152**, 34–40.
21. Waelter, S., Scherzinger, E., Hasenbank, R., Nordhoff, E., Lurz, R., Goehler, H., Gauss, C., Sathasivam, K., Bates, G.P., Lehrach, H. *et al.* (2001) The huntingtin interacting protein HIP1 is a clathrin and alpha-adaptin-binding protein involved in receptor-mediated endocytosis. *Hum. Mol. Genet.*, **10**, 1807–1817.
22. Szebenyi, G., Morfini, G.A., Babcock, A., Gould, M., Selkoe, K., Stenoien, D.L., Young, M., Faber, P.W., MacDonald, M.E., McPhaul, M.J. *et al.* (2003) Neuropathogenic forms of huntingtin and androgen receptor inhibit fast axonal transport. *Neuron*, **40**, 41–52.
23. Gunawardena, S., Her, L.S., Brusch, R.G., Laymon, R.A., Niesman, I.R., Gordesky-Gold, B., Sintasath, L., Bonini, N.M. and Goldstein, L.S. (2003) Disruption of axonal transport by loss of huntingtin or expression of pathogenic polyQ proteins in Drosophila. *Neuron*, **40**, 25–40.
24. Lee, W.C., Yoshihara, M. and Littleton, J.T. (2004) Cytoplasmic aggregates trap polyglutamine-containing proteins and block axonal transport in a Drosophila model of Huntington's disease. *Proc. Natl. Acad. Sci. USA*, **101**, 3224–3229.
25. Trushina, E., Dyer, R.B., Badger, J.D. 2nd, Ure, D., Eide, L., Tran, D.D., Vrieze, B.T., Legendre-Guillemin, V., McPherson, P.S., Mandavilli, B.S. *et al.* (2004) Mutant huntingtin impairs axonal trafficking in mammalian neurons in vivo and in vitro. *Mol. Cell Biol.*, **24**, 8195–8209.
26. Li, H., Li, S.H., Yu, Z.X., Shelbourne, P. and Li, X.J. (2001) Huntingtin aggregate-associated axonal degeneration is an early pathological event in Huntington's disease mice. *J. Neurosci.*, **21**, 8473–8481.
27. Dompierre, J.P., Godin, J.D., Charrin, B.C., Cordelieres, F.P., King, S.J., Humbert, S. and Saudou, F. (2007) Histone deacetylase 6 inhibition compensates for the transport deficit in Huntington's disease by increasing tubulin acetylation. *J. Neurosci.*, **27**, 3571–3583.
28. Block-Galarza, J., Chase, K.O., Sapp, E., Vaughn, K.T., Vallee, R.B., DiFiglia, M. and Aronin, N. (1997) Fast transport and retrograde movement of huntingtin and HAP 1 in axons. *Neuroreport*, **8**, 2247–2251.
29. Braunstein, K.E., Eschbach, J., Rona-Voros, K., Soylu, R., Mikrouli, E., Larmet, Y., Rene, F., Gonzalez De Aguilar, J.L., Loeffler, J.P., Muller, H.P. *et al.* (2010) A point mutation in the dynein heavy chain gene leads to striatal atrophy and compromises neurite outgrowth of striatal neurons. *Hum. Mol. Genet.*, **19**, 4385–4398.
30. Zuccato, C. and Cattaneo, E. (2007) Role of brain-derived neurotrophic factor in Huntington's disease. *Prog. Neurobiol.*, **81**, 294–330.
31. Zuccato, C., Ciammola, A., Rigamonti, D., Leavitt, B.R., Goffredo, D., Conti, L., MacDonald, M.E., Friedlander, R.M., Silani, V., Hayden, M.R. *et al.* (2001) Loss of huntingtin-mediated BDNF gene transcription in Huntington's disease. *Science*, **293**, 493–498.
32. Liot, G., Zala, D., Pla, P., Mottet, G., Piel, M. and Saudou, F. (2013) Mutant Huntingtin alters retrograde transport of TrkB receptors in striatal dendrites. *J. Neurosci.*, **33**, 6298–6309.
33. HD-iPSC-Consortium (2012) Induced pluripotent stem cells from patients with Huntington's disease show CAG-repeat-expansion-associated phenotypes. *Cell Stem Cell*, **11**, 264–278.
34. Li, X., Standley, C., Sapp, E., Valencia, A., Qin, Z.H., Kegel, K.B., Yoder, J., Comer-Tierney, L.A., Esteves, M., Chase, K. *et al.* (2009) Mutant huntingtin impairs vesicle formation from recycling endosomes by interfering with Rab11 activity. *Mol. Cell Biol.*, **29**, 6106–6116.
35. Chung, C.Y., Koprich, J.B., Hallett, P.J. and Isacson, O. (2009) Functional enhancement and protection of dopaminergic terminals by RAB3B overexpression. *Proc. Natl. Acad. Sci. USA*, **106**, 22474–22479.
36. Li, G. (2011) Rab GTPases, membrane trafficking and diseases. *Curr. Drug Targets*, **12**, 1188–1193.
37. Li, X., Sapp, E., Chase, K., Comer-Tierney, L.A., Masso, N., Alexander, J., Reeves, P., Kegel, K.B., Valencia, A., Esteves, M. *et al.* (2009) Disruption of Rab11 activity in a knock-in mouse model of Huntington's disease. *Neurobiol. Dis.*, **36**, 374–383.
38. Dalbem, A., Silveira, C.V., Pedroso, M.F., Breda, R.V., Werne Baes, C.V., Bartmann, A.P. and da Costa, J.C. (2005) Altered distribution of striatal activity-dependent synaptic plasticity in the 3-nitropropionic acid model of Huntington's disease. *Brain Res.*, **1047**, 148–158.
39. Gibson, H.E., Reim, K., Brose, N., Morton, A.J. and Jones, S. (2005) A similar impairment in CA3 mossy fibre LTP in the R6/2 mouse model of Huntington's disease and in the complexin II knockout mouse. *Eur. J. Neurosci.*, **22**, 1701–1712.
40. Kung, V.W., Hassam, R., Morton, A.J. and Jones, S. (2007) Dopamine-dependent long term potentiation in the dorsal striatum is reduced in the R6/2 mouse model of Huntington's disease. *Neuroscience*, **146**, 1571–1580.

41. Milnerwood, A.J. and Raymond, L.A. (2007) Corticostriatal synaptic function in mouse models of Huntington's disease: early effects of huntingtin repeat length and protein load. *J. Physiol.*, **585**, 817–831.
42. Usdin, M.T., Shelbourne, P.F., Myers, R.M. and Madison, D.V. (1999) Impaired synaptic plasticity in mice carrying the Huntington's disease mutation. *Hum. Mol. Genet.*, **8**, 839–846.
43. Schilling, G., Becher, M.W., Sharp, A.H., Jinnah, H.A., Duan, K., Kotzuk, J.A., Slunt, H.H., Ratovitski, T., Cooper, J.K., Jenkins, N.A. *et al.* (1999) Intranuclear inclusions and neuritic aggregates in transgenic mice expressing a mutant N-terminal fragment of huntingtin. *Hum. Mol. Genet.*, **8**, 397–407.
44. Bayram-Weston, Z., Jones, L., Dunnett, S.B. and Brooks, S.P. (2012) Light and electron microscopic characterization of the evolution of cellular pathology in the R6/1 Huntington's disease transgenic mice. *Brain. Res. Bull.*, **88**, 104–112.
45. Bayram-Weston, Z., Jones, L., Dunnett, S.B. and Brooks, S.P. (2012) Light and electron microscopic characterization of the evolution of cellular pathology in YAC128 Huntington's disease transgenic mice. *Brain. Res. Bull.*, **88**, 137–147.
46. Gabery, S., Sajjad, M.U., Hult, S., Soylu, R., Kirik, D. and Petersen, A. (2012) Characterization of a rat model of Huntington's disease based on targeted expression of mutant huntingtin in the forebrain using adeno-associated viral vectors. *Eur. J. Neurosci.*, **36**, 2789–2800.
47. Tabrizi, S.J., Scahill, R.I., Owen, G., Durr, A., Leavitt, B.R., Roos, R.A., Borowsky, B., Landwehrmeyer, B., Frost, C., Johnson, H. *et al.* (2013) Predictors of phenotypic progression and disease onset in premanifest and early-stage Huntington's disease in the TRACK-HD study: analysis of 36-month observational data. *Lancet Neurol.*, **12**, 637–649.
48. Slow, E.J., van Raamsdonk, J., Rogers, D., Coleman, S.H., Graham, R.K., Deng, Y., Oh, R., Bissada, N., Hossain, S.M., Yang, Y.Z. *et al.* (2003) Selective striatal neuronal loss in a YAC128 mouse model of Huntington disease. *Hum. Mol. Genet.*, **12**, 1555–1567.
49. Lastres-Becker, I., Hansen, H.H., Berrendero, F., De Miguel, R., Perez-Rosado, A., Manzanares, J., Ramos, J.A. and Fernandez-Ruiz, J. (2002) Alleviation of motor hyperactivity and neurochemical deficits by endocannabinoid uptake inhibition in a rat model of Huntington's disease. *Synapse*, **44**, 23–35.
50. Reiner, A., Dragatsis, I. and Dietrich, P. (2011) Genetics and neuropathology of Huntington's disease. *Int. Rev. Neurobiol.*, **98**, 325–372.
51. Sotrel, A., Paskevich, P.A., Kiely, D.K., Bird, E.D., Williams, R.S. and Myers, R.H. (1991) Morphometric analysis of the prefrontal cortex in Huntington's disease. *Neurology*, **41**, 1117–1123.
52. Al-Abdulla, N.A. and Martin, L.J. (1998) Apoptosis of retrogradely degenerating neurons occurs in association with the accumulation of perikaryal mitochondria and oxidative damage to the nucleus. *Am. J. Pathol.*, **153**, 447–456.
53. Deng, Y.P., Wong, T., Bricker-Anthony, C., Deng, B. and Reiner, A. (2013) Loss of corticostriatal and thalamostriatal synaptic terminals precedes striatal projection neuron pathology in heterozygous Q140 Huntington's disease mice. *Neurobiol. Dis.*, **60**, 89–107.
54. Cha, J.H., Kosinski, C.M., Kerner, J.A., Alsdorf, S.A., Mangiarini, L., Davies, S.W., Penney, J.B., Bates, G.P. and Young, A.B. (1998) Altered brain neurotransmitter receptors in transgenic mice expressing a portion of an abnormal human huntington disease gene. *Proc. Natl. Acad. Sci. USA*, **95**, 6480–6485.
55. Carter, R.J., Lione, L.A., Humby, T., Mangiarini, L., Mahal, A., Bates, G.P., Dunnett, S.B. and Morton, A.J. (1999) Characterization of progressive motor deficits in mice transgenic for the human Huntington's disease mutation. *J. Neurosci.*, **19**, 3248–3257.
56. Nicniocaill, B., Haraldsson, B., Hansson, O., O'Connor, W.T. and Brundin, P. (2001) Altered striatal amino acid neurotransmitter release monitored using microdialysis in R6/1 Huntington transgenic mice. *Eur. J. Neurosci.*, **13**, 206–210.
57. Loh, D.H., Kudo, T., Truong, D., Wu, Y. and Colwell, C.S. (2013) The Q175 mouse model of Huntington's disease shows gene dosage- and age-related decline in circadian rhythms of activity and sleep. *PLoS One*, **8**, e69993.
58. Morton, A.J. (2013) Circadian and sleep disorder in Huntington's disease. *Exp. Neurol.*, **243**, 34–44.
59. Andre, V.M., Fisher, Y.E. and Levine, M.S. (2011) Altered balance of activity in the striatal direct and indirect pathways in mouse models of Huntington's disease. *Front. Syst. Neurosci.*, **5**, 46.
60. Callahan, J.W. and Abercrombie, E.D. (2011) In vivo dopamine efflux is decreased in striatum of both fragment (R6/2) and full-Length (YAC128) transgenic mouse models of Huntington's disease. *Front. Syst. Neurosci.*, **5**, 61.
61. Gorlich, D. and Mattaj, I.W. (1996) Nucleocytoplasmic transport. *Science*, **271**, 1513–1518.
62. Rubinsztein, D.C. and Carmichael, J. (2003) Huntington's disease: molecular basis of neurodegeneration. *Expert. Rev. Mol. Med.*, **5**, 1–21.
63. Waldron-Roby, E., Ratovitski, T., Wang, X., Jiang, M., Watkin, E., Arbez, N., Graham, R.K., Hayden, M.R., Hou, Z., Mori, S. *et al.* (2012) Transgenic mouse model expressing the caspase 6 fragment of mutant huntingtin. *J. Neurosci.*, **32**, 183–193.
64. Thompson, L.M., Aiken, C.T., Kaltenbach, L.S., Agrawal, N., Illes, K., Khoshnan, A., Martinez-Vincente, M., Arrasate, M., O'Rourke, J.G., Khashwji, H. *et al.* (2009) IKK phosphorylates Huntingtin and targets it for degradation by the proteasome and lysosome. *J. Cell. Biol.*, **187**, 1083–1099.
65. Ikenaka, K., Kawai, K., Katsuno, M., Huang, Z., Jiang, Y.M., Iguchi, Y., Kobayashi, K., Kimata, T., Waza, M., Tanaka, F. *et al.* (2013) dnc-1/dynactin 1 knockdown disrupts transport of autophagosomes and induces motor neuron degeneration. *PLoS One*, **8**, e54511.
66. Pilling, A.D., Horiuchi, D., Lively, C.M. and Saxton, W.M. (2006) Kinesin-1 and Dynein are the primary motors for fast transport of mitochondria in Drosophila motor axons. *Mol. Biol. Cell*, **17**, 2057–2068.
67. Eschbach, J. and Dupuis, L. (2011) Cytoplasmic dynein in neurodegeneration. *Pharmacol. Ther.*, **130**, 348–363.
68. Caviston, J.P., Ross, J.L., Antony, S.M., Tokito, M. and Holzbaur, E.L. (2007) Huntingtin facilitates dynein/dynactin-mediated vesicle transport. *Proc. Natl. Acad. Sci. USA*, **104**, 10045–10050.
69. Altar, C.A., Cai, N., Bliven, T., Juhasz, M., Conner, J.M., Acheson, A.L., Lindsay, R.M. and Wiegand, S.J. (1997) Anterograde transport of brain-derived neurotrophic factor and its role in the brain. *Nature*, **389**, 856–860.
70. Giampa, C., Montagna, E., Dato, C., Melone, M.A., Bernardi, G. and Fusco, F.R. (2013) Systemic delivery of recombinant brain derived neurotrophic factor (BDNF) in the R6/2 mouse model of Huntington's disease. *PLoS One*, **8**, e64037.
71. Samadi, P., Boutet, A., Rymar, V.V., Rawal, K., Maheux, J., Kvann, J.C., Tomaszewski, M., Beaubien, F., Cloutier, J.F., Levesque, D. *et al.* (2013) Relationship between BDNF expression in major striatal afferents, striatum morphology and motor behavior in the R6/2 mouse model of Huntington's disease. *Genes Brain Behav.*, **12**, 108–124.
72. Gokce, O., Runne, H., Kuhn, A. and Luthi-Carter, R. (2009) Short-term striatal gene expression responses to brain-derived neurotrophic factor are dependent on MEK and ERK activation. *PLoS One*, **4**, e5292.
73. Lu, B., Nagappan, G., Guan, X., Nathan, P.J. and Wren, P. (2013) BDNF-based synaptic repair as a disease-modifying strategy for neurodegenerative diseases. *Nat. Rev. Neurosci.*, **14**, 401–416.
74. Murmu, R.P., Li, W., Holtmaat, A. and Li, J.Y. (2013) Dendritic spine instability leads to progressive neocortical spine loss in a mouse model of Huntington's disease. *J. Neurosci.*, **33**, 12997–13009.
75. Nithianantharajah, J. and Hannan, A.J. (2012) Dysregulation of synaptic proteins, dendritic spine abnormalities and pathological plasticity of synapses as experience-dependent mediators of cognitive and psychiatric symptoms in Huntington's disease. *Neuroscience*, **251**, 66–74.
76. DiProspero, N.A., Chen, E.Y., Charles, V., Plomann, M., Kordower, J.H. and Tagle, D.A. (2004) Early changes in Huntington's disease patient brains involve alterations in cytoskeletal and synaptic elements. *J. Neurocytol.*, **33**, 517–533.
77. Wojtowicz, A.M., Dvorzhak, A., Semtner, M. and Grantyn, R. (2013) Reduced tonic inhibition in striatal output neurons from Huntington mice due to loss of astrocytic GABA release through GAT-3. *Front. Neural Circuits*, **7**, 188.
78. Heikkinen, T., Lehtimaki, K., Vartiainen, N., Puolivali, J., Hendricks, S.J., Glaser, J.R., Bradaia, A., Wadel, K., Touller, C., Kontkanen, O. *et al.* (2012) Characterization of neurophysiological and behavioral changes, MRI brain volumetry and 1H MRS in zQ175 knock-in mouse model of Huntington's disease. *PLoS One*, **7**, e50717.
79. Castillo, P.E., Janz, R., Sudhof, T.C., Tzounopoulos, T., Malenka, R.C. and Nicoll, R.A. (1997) Rab3A is essential for mossy fibre long-term potentiation in the hippocampus. *Nature*, **388**, 590–593.

80. Smith, R., Klein, P., Koc-Schmitz, Y., Waldvogel, H.J., Faull, R.L., Brundin, P., Plomann, M. and Li, J.Y. (2007) Loss of SNAP-25 and rabphilin 3a in sensory-motor cortex in Huntington's disease. *J. Neurochem.*, **103**, 115–123.
81. Stowers, R.S. and Isacoff, E.Y. (2007) Drosophila huntingtin-interacting protein 14 is a presynaptic protein required for photoreceptor synaptic transmission and expression of the palmitoylated proteins synaptosome-associated protein 25 and cysteine string protein. *J. Neurosci.*, **27**, 12874–12883.
82. Cattaneo, E., Rigamonti, D., Goffredo, D., Zuccato, C., Squitieri, F. and Sipione, S. (2001) Loss of normal huntingtin function: new developments in Huntington's disease research. *Trends Neurosci.*, **24**, 182–188.
83. Hu, D., Cao, Y., He, R., Han, N., Liu, Z., Miao, L. and Yin, J. (2012) Schizandrin, an antioxidant lignan from Schisandra chinensis, ameliorates Abeta1–42-induced memory impairment in mice. *Oxid. Med. Cell Longev.*, **2012**, 721721.
84. Deacon, R.M. (2006) Assessing nest building in mice. *Nat. Protoc.*, **1**, 1117–1119.